A Study on the Feasibility of 3D Micromachining and Micro-Molding Using Nanosecond Laser

Shayan Mohammadi Pour Khajani

A Thesis

In the Department

of

Mechanical, Industrial and Aerospace Engineering

Presented in Partial Fulfillment of the Requirements

For the Degree of Master of Applied Science at

Concordia University

Montreal, Quebec, Canada

March 2022

CONCORDIA UNIVERSITY

SCHOOL OF GRADUATE STUDIES

This is to certify that this thesis is prepared

By: Shayan Mohammadi Pour Khajani

Entitled: A Study on the Feasibility of 3D Micromachining and Micro-Molding Using Nanosecond Laser

and submitted in partial fulfillment of the requirements for the degree of

Master of Applied Science («Mechanical Engineering»)

complies with the regulations of the University and meets the accepted standards with respect to originality and quality.

Signed by the final examining committee:

_____Chair
Dr. Javad Dargahi

_____ Examiner
Dr. Javad Dargahi

_____ Examiner
Dr. Anjan Bhowmick

_____Thesis Supervisor
Dr. Sivakumar Narayanswamy

Approved by _____

Dr. Sivakumar Narayanswamy

Chair of Department or Graduate Program Director

_____ «Examination_Date» _____

Dr. Mourad Debbabi

Dean of Gina Cody School of Engineering and Computer Science

Abstract

A Study on the Feasibility of 3D Micromachining and Micro-Molding Using Nanosecond Laser

Shayan Mohammadi Pour Khajani

Today, miniaturization is evident in almost every field of manufacturing. Laser micromachining can produce high-precision microstructures and micro-components. The current project proposes an air jet-assisted laser micromachining for the fabrication of 3D microstructures and micro-molds. In the developed laser micromachining system, MATLAB algorithms were used to control the galvoscanner mirrors to direct the laser beam in the x and y-directions. Further, an adjustable stage was used to enable the movement in z-direction to facilitate 3D laser micromachining.

Laser parameters such as overlap, laser power, and the number of pulses were varied to investigate the performance. The results were analyzed in terms of machining depth, surface roughness, and machining accuracy to obtain optimum parameters for micromachining. For the micromachining setup developed as part of this work, a laser with 532 nm wavelength, 1.1 W power, 80% overlap between spots, and 400 pulses per spot provided optimum results, a roughness of 1.89 µm, and depth of 21.31 µm. Concordia logo was selected as a complex shape to perform a 2D micromachining. This experiment was conducted with the optimum parameters on four different scales starting from 4 mm down to 1 mm. The aim was to find how accurate is the micromachining to generate features on small scales considering the spot size is 60 µm in our setup.

The goal of this study is to present a high-precision 3D laser micromachining system. An experiment was designed to generate a 3D pyramid to ascertain the feasibility. While machining layer-by-layer, melt debris presented a significant challenge. To overcome this, an air jet was directed towards the machining area to clear the melt debris in situ. The results were investigated by interferometer and confocal microscopes in terms of machining depth and surface roughness in each layer.

Subsequently, a 3 mm diameter gear was selected as a complex shape to investigate the ability to fabricate features such as corners and edges accurately. In the final step of this research, the pyramid and gear were used as molds to fabricate the polydimethylsiloxane (PDMS) structures. The micrometric features such as corners and edges were accurately molded.

Acknowledgments

I would like to sincerely express my deepest appreciation and thankfulness to my supervisor Dr. Sivakumar Narayanswamy for his unparalleled support, expert guidance, and unfaltering faith in me throughout my graduate studies at Concordia University.

I am thankful and appreciate my colleague Dr. Hamid Ebrahimi Orimi for his continuous encouragement, as well as his unselfish willingness to help me with the technical issues and mental support. Also, I would like to thank my fellow graduate students, Mrs. Mahta Nazemi and Mrs. Sevin Samadi for their friendly support during hard times.

I would like to express my sincerest thanks to Mrs. Fourogh Khani for her unselfish support, which enabled me to overcome the most difficult times in my life.

Finally, I wish to express my sincere gratitude to my dear parents, Mr. Morteza Mohammadi Pour Khajani and Mrs. Fariba Enayat Jou, who have been continuously supporting my education and intellectual development for a long time, without whom I could not have accomplished this achievement in life. Also, I would like to thank my only dear sister, Mrs. Shadi Mohammadi Pour Khajani, who has always supported me on difficult days.

Dedication

To my father

Who supported me in every way in my life,

And taught me to be strong and independent

To my mother

My best teacher

who has been a source of motivation and

strength in hard moments

Table of Contents

List of Figures

List of Tables

Nomenclature

f	Focal length of lens	mm
λ	Wavelength of the laser	Nm
D	Diameter of laser before the lens	Mm
d	Laser spot diameter	μ
φ	Rotation angle of the galvo-mirror	Degree
L	Length of laser scan	Mm
α	Galvo scanner motor angle in x direction	Degree
β	Galvo scanner motor angle in y direction	Degree
O_v	Overlap	--
O_p	Overlap percentage	--
V	Voltage	Volt
W	Laser power	Watt

CHAPTER 1. INTRODUCTION

1.1 Micromachining

Today, miniaturization is a trend evident in almost all production fields such as automotive, aerospace, photonics, renewable energy, and medical instruments, to name a few. Due to the complexity of these micro products, several micro-machining processes are usually required to deliver a high-quality product. Various methods such as lithography, chemical or plasma etching, printing, molding, etc., were introduced to produce components with miniature feature sizes in both organic and inorganic materials and even in complex three-dimensional (3D) shapes [1].

Also, several hybrid micromachining techniques have been developed for improving surface roughness, tool life, and machining accuracy. These techniques are extremely beneficial to fabricate complex micro-parts on hard and multi-materials. Typically, hybrid micromachining can be divided into assisted micromachining and combined micromachining.

In assisted micromachining, a variety of energies, such as ultrasonic vibration, laser, fluid, magnetic field, etc., merge to improve the micromachining process. In combined micromachining, all machining processes such as electrical and electrochemical machining, etc., work simultaneously to do the machining and affect the machining zone. This technique improves the machining potential to produce complex shapes in terms of material removal rate, surface integrity, and machining accuracy at a relatively high speed [2]. In the following, some micromachining investigations are reviewed.

1.1.1 Electrochemical Micromachining

Electrochemical micromachining (ECMM) is an unconventional micromachining process that offers fabricating of micro-holes, micro-cavities, and micro-channels on conductive and hard materials with a high aspect ratio. Also, it offers promising machining performance in terms of high surface finish, no tool wear, and the absence of thermally induced defects. The principle of material removal in this method is the anodic dissolution of the workpiece. However, in ECMM the purpose is to localize the material removal to control the shape precisely. ECMM provides micromachining without thermal defects such as the heat-affected zone (HAZ), fabrication of complex micro-shapes, high surface finishes, and no tool wear. This technique has some limitations such as inability to machine non-conductive materials, high production costs, and corrosion of the equipment [3].

Maniraj et al presented a method of electrolyte heating to improve the performance of the micromachining process. Figure 1-1 shows their modified electrochemical micromachining setup and a schematic of tool electrode-heating system. This technique shows that electrolyte temperature plays a critical role as an additional variable in enhancing the machining process and increasing the reaction rate. The electrode-heating increases the heat of the electrolyte solution, thereby increasing material removal rate (MRR). Moreover, a higher voltage level improves chemical dissolution of the matrix material and increases the MRR [4].

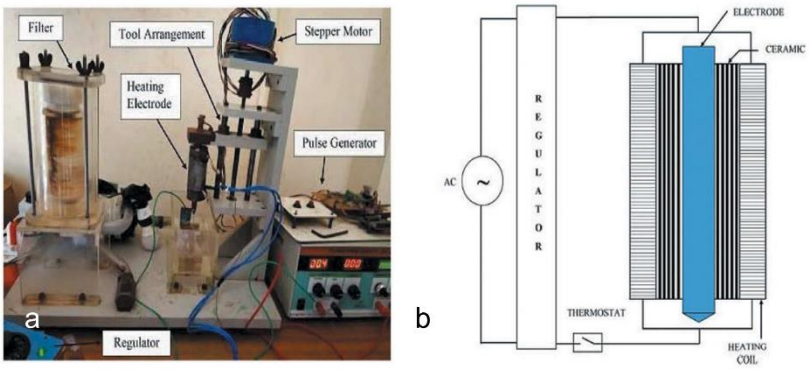

Figure 1-1Modified Electrochemical Micro-Machining Setup & (b) Tool electrode-heating system [4].

The motion mode, machining rate, and tool gap can affect micromachining quality. Ye et al. have shown that the shorter the applied voltage pulse is, the smaller the groove size could be (Figure 1-2 (a)). Additionally, they found that the longer the distance between the tool and workpiece, the wider the groove (Figure 1-2 (b)). On the other hand, the groove width decreases as the machining moving rate increases (Figure 1-2 (c)) [5].

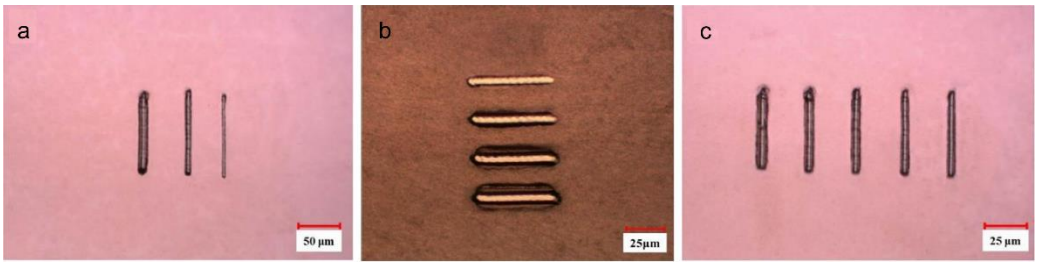

Figure 1-2. (a) The machining with different pulse periods, (b) The machining with different tool-workpiece distances (c) the groove width with different moving rates [5].

The ECMM parameters mainly affect the surface roughness. This occurs because electrolytic products usually accumulate easily in the machining gap, resulting in a rough surface. Xu et al

presented the optimal cathode traveling speed to improve the surface roughness. Also, an increase in the frequency and amplitude of anode vibration enhances the surface roughness. Furthermore, they found that voltage variation can affect the roughness quality, and the roughness decreases between voltages 4 and 6 V. Figure 1-3 depicts the surface roughness with and without cathode traveling [6].

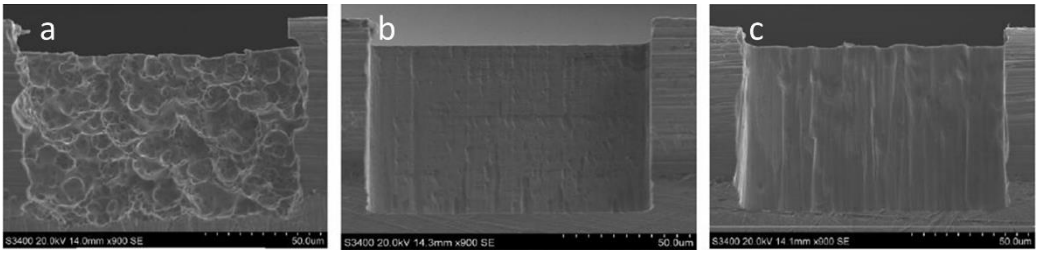

Figure 1-3. (a) Without cathode traveling. (b) Amplitude = 100 µm and speed = 400 µms^{-1}. (c) Amplitude = 100 µm and speed = 800 µms^{-1} [6].

1.1.2 Waterjet Micromachining

Waterjet micromachining technology is a high-pressure waterjet cutting system. In 1980, Dr. Hashish invented the abrasive waterjet (AWJ) to cut wide range of industrial materials such as metals and non-metals by adding the abrasive to the plain of waterjet. The main reason for the widespread use of this technique is its machining versatility and the lack of thermal distortion on the workpiece at the cutting zone. On the other hand, AWJ has some fundamental or functional limitations such as low depth of penetration, low material removal rate, rough quality surface, taper profile, and striation formation [7].

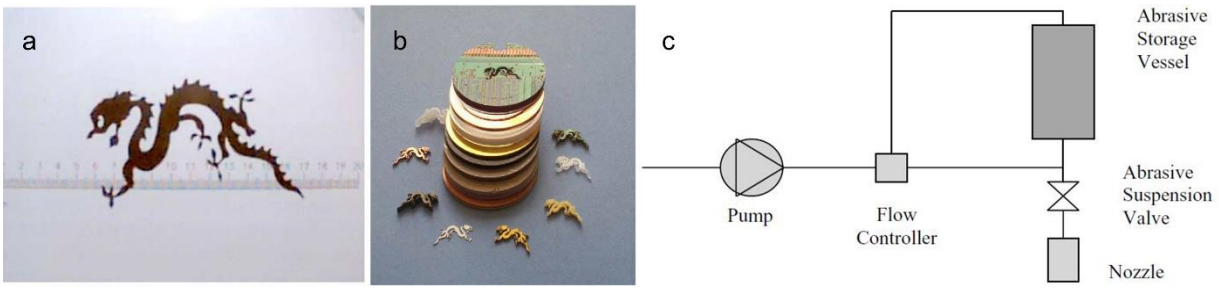

Figure 1-4. (a) Profile from 50 µm thick stainless steel, cut with 300 nm abrasive. (b) Examples of materials cut with 40–60 µm jets. (c) Flow circuit [8].

Miller developed a suspension system to improve their abrasive waterjet micromachining performance that can mill, drill, and cut metal and non-metal materials. Figure 1-4 shows the details of the parts that could be machined by the abrasive waterjet micromachining and the

schematic of developed system. Further, they developed valves to allow the AWJ to drill several holes per second. They found that the abrasive waterjets generated by the suspension method can provide higher machining variables than conventional systems but at the micro-level [8].

Liu studied the performance of abrasive waterjets on thin metal by cutting different geometric shapes and font sets using several orifice/mixing tube diameter ratios and waterjets. Based on the results, the smallest achievable groove width by AWJ is about 200µm. The smallest achievable groove width is possible by AWJ setup, and it is about 200µm. WJ-machining can produce grooves less than 200µm width on thin or soft metals like aluminum, but it offers lower quality than AWJ. A novel process was developed to work simultaneously with the AWJ nozzle for machining very thin slots. Figure 1-5 illustrates a comparison of machining with the AWJs and the novel abrasive waterjet/stencil-aided waterjet stage (AWJ/SAWS) combination [9].

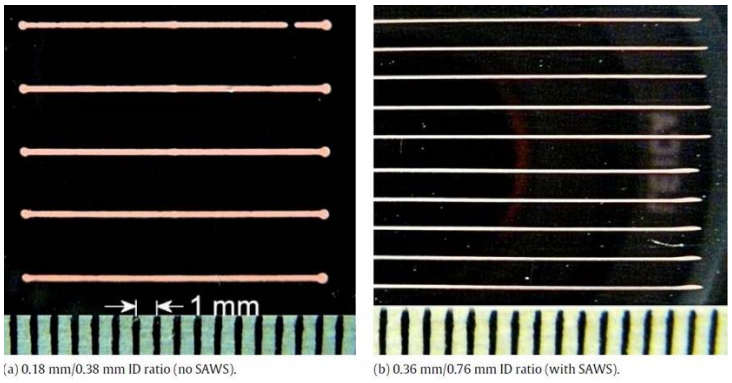

Figure 1-5. Machining with the AWJs and the novel AWJ/SAWS combination [9].

1.1.3 Bulk Micromachining

Bulk micromachining is a method of fabricating micro-electro-mechanical systems (MEMS) on semiconductor substrates using selective etching inside a substrate. There are two types of bulk micromachining techniques: wet and dry etching. The wet etching process is a method for removing materials from a wafer by using chemicals or etchants and dry etching is a process that the substrate material removes by applying plasmas or etchant gasses. Wet and dry etchings are extensively used for fabricating microscale structures such as microchannels and microcavities [10]. Important advantages of this technique are the fabrication of complex 2.5D structures, and simplicity. However, it has some limitations such as needs clean room, need masks, and dimensional control at the micron level [11].

Yoon et al investigated wet bulk micromachining of Si by metal-assisted chemical etching (MaCE). They found that the generation of hydrogen bubbles in DI-based etchant causes a non-uniform surface, and they can reduce the bubble formation by increasing the wettability of the etchant. Therefore, a low surface tension co-solvent (ethanol) was added to the conventional etchant to improve its wettability and prevent bubble formation on the surface. Bubble elimination results in uniform etch rates across the surface and prevent premature cracking of the catalyst metal layer. On the other hand, the addition of ethanol may decrease the etch rate because it can limit the access of etchant onto the metal surface [12].

Kim et al designed a magnetically guided metal-assisted chemical etching (MACE) process to improve the etching performance in the bulk micromachining of Si. A triple layer metal catalyst (Au, Fe, Au) was deposited on Si substrate. As shown in Figure 1-6, a magnet was placed under the substrate to speed and guide the etching direction by a magnetic pulling force. As well, this method allowed them to fabricate the curved microstructures in the desired direction by moving the magnet. Finally, an annealing process was performed on the catalyst to obtain a rougher surface and improve the ferromagnetic properties, which increases the etching rate for magnetically guided MACE [13].

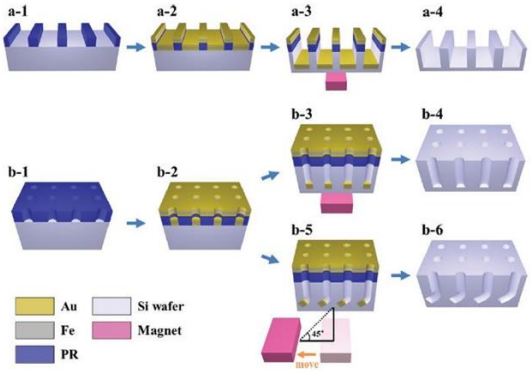

Figure 1-6. Micromachining of bulk Si with magnetically guided MACE [13].

Hoshian et al. demonstrated a non-lithographic and vacuum-free method to pattern silicone. A hybrid method (INKMAC) was presented which is the combination of inkjet printing and metal-assisted chemical etching (MACE). Figure 1-7 shows scanning electron microscopy (SEM) images of INKMAC process flow with corresponding. Silver commercial ink was considered to create the catalyst patterns for MACE on the silicon surface. This process creates a set of silicon nanowires in the shape of the inkjet printer pattern. Also, they demonstrated cavities with resolution down to

30 µm diameters and 50 µm channels widths which are sufficient for many applications such as MEMS devices, etc., [14].

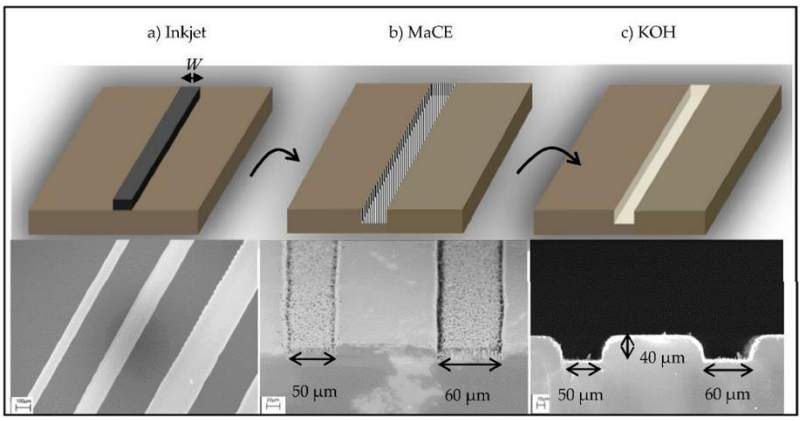

Figure 1-7. Process flow with corresponding SEM images, (a) Inkjetting silver nanoparticles; (b) Metal assisted chemical etching (MaCE); (c) Potassium hydroxide (KOH) etching of silicon nanowires to open the channels [14].

1.1.4 Micro-texturing

Texturing is a method of changing the surface characteristic such as self-cleaning, load capacity, reducing the coefficient of friction so as to enhance its performance without changing the original properties. Various methods exist for generating textured surfaces such as laser texturing, through-mask electrochemical micromachining, lithography, micro or nano casting, etc. The disadvantages of these methods are the lack of a smooth surface, and they are limited to 2D micromachining [15].

Jana D. Abou Ziki et al designed an experiment to create a micro-texturing channel on glass using spark-assisted chemical engraving (SACE) and investigate its utility for microfluidics and biotechnology. It was illustrated that electrochemical discharged machining can be used as a tool to create surface texturing a glass microchannel. Figure 1-8 indicates a schematic of (SACE) machining setup and tool-electrode geometry. Some parameters like tool travel speed, voltage, and tool gap can affect the experiment results directly. Variation of electrolyte concentration can significantly affect surface texture. Figure 1-9 shows the viscosity of the electrode and its important influence in channel texturing. With an increase in electrode concentration, the texturing pattern changes from branched feathery to smooth spongy (porous). As shown in Figure 1-9 (e), since the thermal conductivity of electrolyte increases above 30wt%, the microchannels cracks at 30wt% and 40wt% NaOH electrolyte solutions [16].

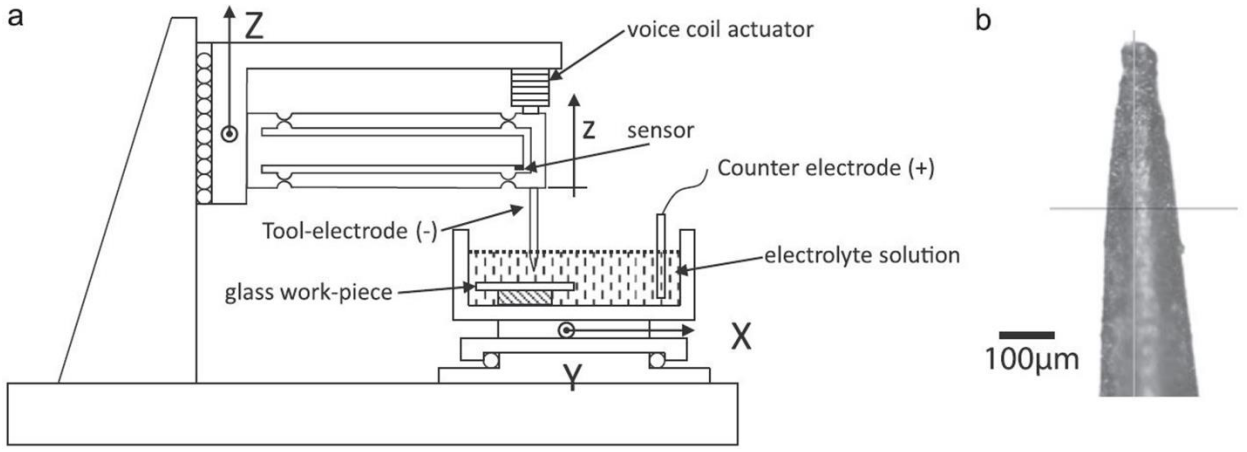

Figure 1-8. (a) Schematic of (SACE) machining setup (b) Tool-electrode geometry [16].

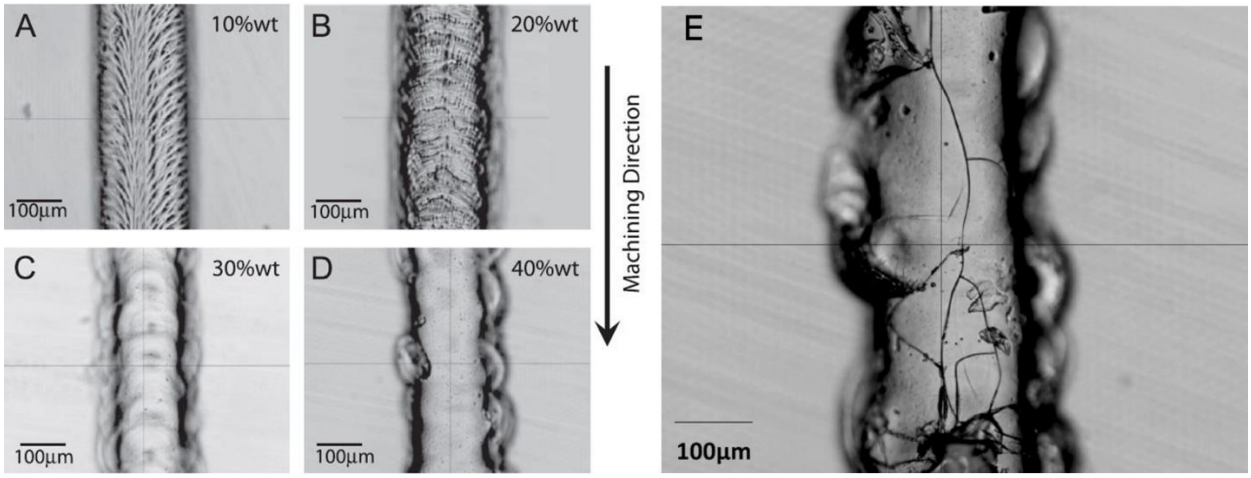

Figure 1-9. Machined channels at a voltage equal to 28V and a speed equal to 5 mm/s while using different NaOH concentrations (10wt%, 20wt%, 30wt% and, 40wt% NaOH) [16].

In this section, a brief review was carried out on the different micromachining techniques such as electrochemical micromachining (ECMM), waterjet micromachining, bulk micromachining (wet and dry etching), and micro-texturing. Based on the literature review, the weakness and the capabilities of each technique to fabricate the micro-componenets were identified. In the next section, a brief review of different techniques in laser micromachining was carried out.

1.2 Laser Micromachining

Laser micromachining is a non-contact machining process, which can fabricate a high precision microstructure and micro-components ranging up to 500µm with the help of lasers. This technique

offers higher precision, consistent results, faster throughput, higher yields, and lower manufacturing cost in comparison to the other micromachining techniques. Laser micromachining works by ablating (removal of material thermally or using photochemical erosion) materials. Laser ablation is dependent upon the intensity, wavelength, and proper shape. Lasers with shorter wavelengths, such as Ultraviolet rays, result in a lower peripheral heating. The pulsed laser produces high peak power at lower average power consumption. Due to the short pulse duration and high peak power of nano/pico/femtosecond lasers, they generate low heat affected zone, which provides highly accurate micromachining. Figure 1-10 depicts the advancement of laser micromachining [17]. In the following, some laser micromachining investigations were reviewed.

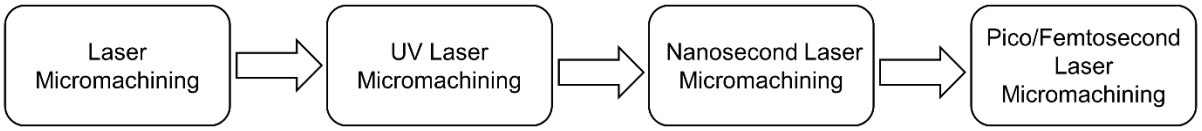

Figure 1-10. Advancement in laser micromachining [17].

Lern et al. investigated the effect of line intensity and line overlap on production of homogeneous microstructures (pillow-like and bumpy-like) by using a 10 kHz femtosecond laser. They found that the pillow-like structures created at a wide range of overlap at moderate intensities and bumpy-like structures created at a tighter range of overlap at higher intensities. Also, simulation shows that the pillow-like structures created at a flat intensity profile, while bumpy structures are produced with a wavy profile [18].

Charee et al. presented an ultrasonic-assisted laser ablation to eliminate cut debris and bubble underwater. The ultrasound vibrates the water during laser micromachining to atomize the bubble and flush away debris from the machining area. Figure 1-11 depicts a schematic of ultrasonic-assisted underwater laser ablation system. The results illustrate that micromachining under ultrasonic condition can produce a narrower cut and smaller bubbles. An increase in travel speed decreases the groove width for all ultrasonic conditions. Moreover, the machining depth increases with the ultrasonic power and ultrasonic frequency. This could be explained by collapsing of cavitation bubble in water by the ultrasound. Under high ultrasonic power and frequency, a smaller cavitation bubbles can be created, which reduce the laser beam refraction and increase laser beam penetration, resulting in deeper machining. Furthermore, a higher water flow rate expels the laser-

molten material from machining area and prevent the blocking of laser beam and improves the machining efficiency [19].

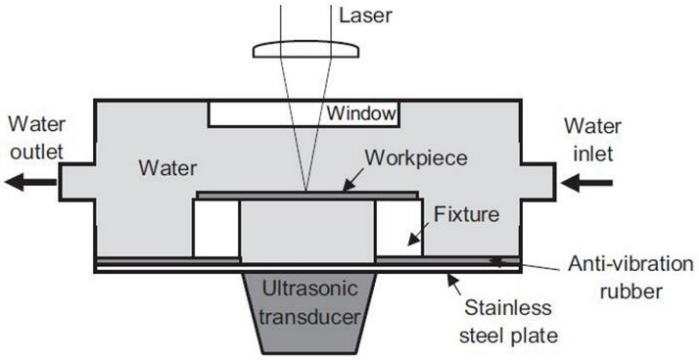

Figure 1-11. Ultrasonic-assisted underwater laser ablation in a closed chamber with water flow [19].

Chang et al examined the effects of static and dynamic magnetic fields to assist the laser micromachining. Two different arrangements magnet (single pair magnet and multiple pair) were designed for generating a static magnetic field. Also, three different magnet positions, including 2 mm below the sample, equal to the sample, and 2 mm above the sample was considered for laser micromachining. Positioning the magnet 2 mm above the sample showed the highest micromachining efficiency, while the inlet diameter was the smallest at the positioning of 2 mm below the sample. It was found that the machining depth with the assistance of the magnetic field was deeper than the depth in the absence of magnetic field. Furthermore, the deepest hole was created by the single-pair magnet.

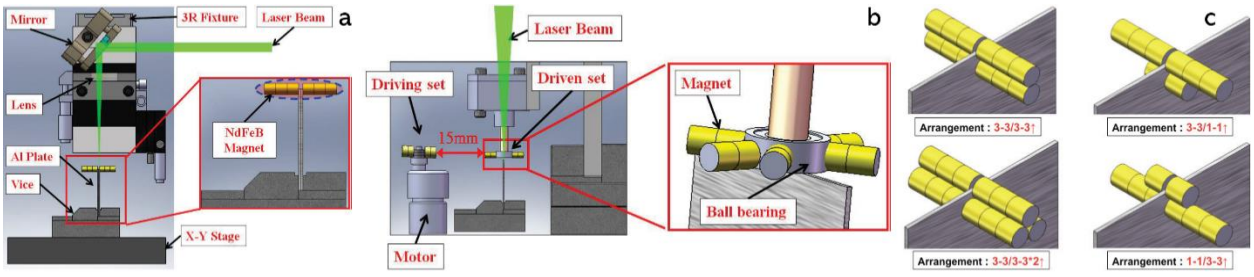

Figure 1-12. (a) Schematic of the experimental setup with a static magnetic field (b) Schematic of the experimental setup with a dynamic magnetic field (c) Vertical arrangement of multiple magnetic pairs [20].

In multiple magnet pairs, the arrangement of 3-3/3-3*2↑ provided the best result to both the machining efficiency and the inlet diameter. Figure 1-12 (c) shows the arrangements of multiple

magnetic pairs. In the dynamic magnetic field, rotational assembled magnets generate a smooth magnetic field which improves the roundness of the inlet and decreases the HAZ [20].

Chkalov et al studied the coating of a quartz substrate with a thin titanium film via femtosecond laser micromachining. First, by evaporating the titanium via laser beam a thin titanium film was coated on the quartz substrate in the vacuum chamber. Coating deposition depends on a various parameter, such as the speed of laser beam along the surface, the duration of scanning and distance of the sample from substrate. Micromachining was performed with a developed hardware-software complex of femtosecond laser micromachining. Figure 1-13 shows a schematic of geometry of the titanium film deposition and result of the micromachining the substrate coating of given geometry [21].

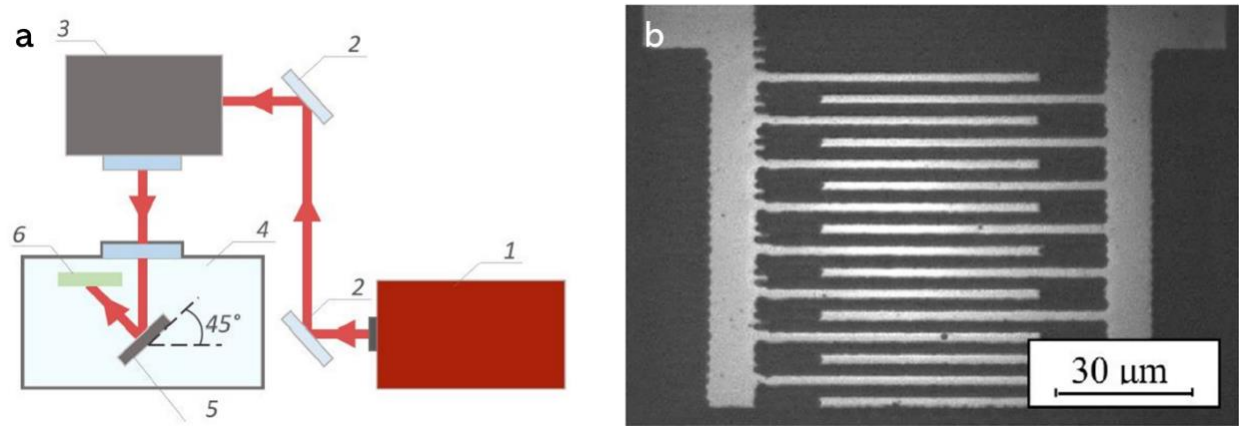

Figure 1-13. (a) Geometry of the titanium film deposition experiment. (b) Optical image of result of the micromachining the substrate coating in the form of element of given geometry [21].

Loor has presented a laser writing method by a synchronized polygon scanning system instead of using galvanometers to enable a writing speed of 50 m/s or higher with ultra-short lasers. First, a fixed galvanometer deflects the laser beam and makes a one-direction motion towards the polygon scanner. Then, the rotating polygon scanner makes the secondary motion which is perpendicular to the line scanned to perform a line-by-line 2-dimensional scanning. Figure 1-14 depicts a schematic of the synchronized polygon scanning system. Using such a scanning system, Loor was able to use ultra-short-pulsed laser for high-speed micromachining [22].

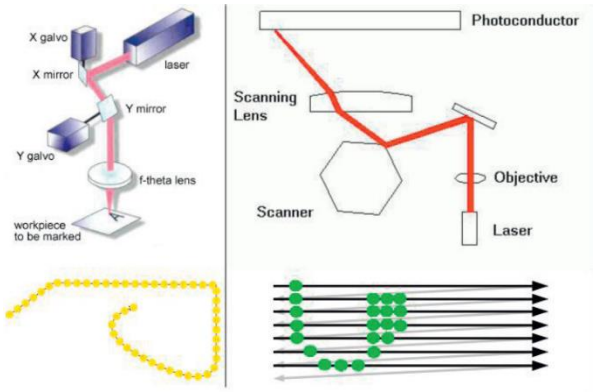

Figure 1-14. Galvo versus polygon scanning [22].

Nayak et al presented a simple and low-cost laser micro texturing fabricate a superhydrophobic surface by directly replicating micro/nanostructures on polydimethylsiloxane (PDMS) by ultrafast laser. Two types of substrates were investigated in this study: Si and Ti which were laser microtextured by Ti-Sapphire ultrafast laser system (tunable laser that with 800 nm wavelength). First, the samples were textured under the laser beam to achieve a uniform surface to be used for replication of micro/nano structures on to PDMS. Surface roughness plays an important role in producing superhydrophobic surfaces. Figure 1-15 illustrates the images of water drop on PDMS plane and replicated surfaces. As is clear, the superhydrophobic surface make larger contact angle with the water drop and this method enables surfaces to reach CA > 154° [23].

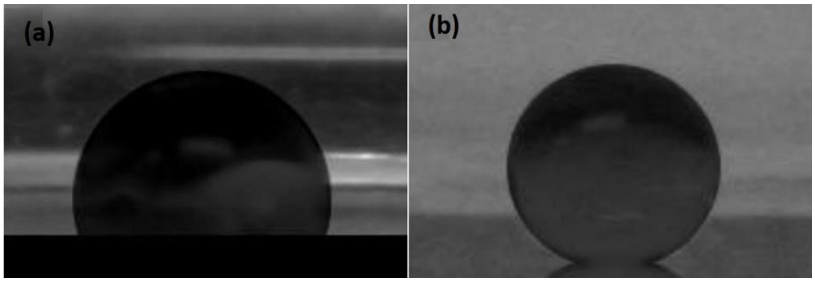

Figure 1-15. SEM image of replicated micro/nano structures on PDMS surfaces: (a) plane PDMS (b) micro/nano structure replicated PDMS surface [23].

Martínez-Calderon et al used a femtosecond (fs) laser micro/nano machining technology to modify the surface structures aiming at controlling the cell adhesion and migration. The investigations show the cells tend to migrate align to the laser-induced nanopatterns oriented in a specific direction. As shown in Figure 1-16, laser-Induced Periodic Surface Structures (LIPSS) nanopatterns with different orientations were fabricated on stainless steel substrates to study the

cell behavior. The results show that changing the overall shape of the micro/nano textured patterns, including their geometry and orientation, can affect cell distribution and migration dramatically. In all, surface texturing by femtosecond laser provided a precise control over the surface nano-patterning process [24].

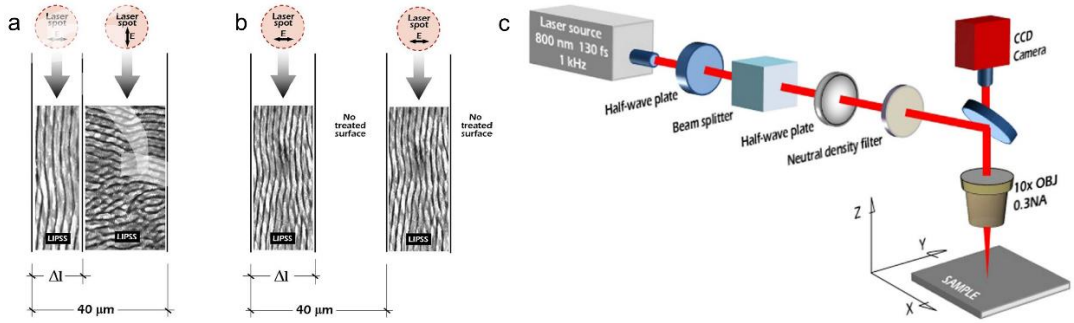

Figure 1-16. Surface structure oriented perpendicularly by rotating the laser beam polarization. (b) Surface structure alternating vertical LIPSS nanopatterns and non-treated microstrips. (c) Schematic layout of the femtosecond laser machining setup [24].

Chang et al studied a direct and quick single-step machining method by using the femtosecond laser as a reliable, quick, and competitive alternative tool to fabricate two-dimensional array patterns on the sapphire surface. Since the threshold fluence is the minimum required energy per unit surface to create a change on the sapphire surface, it is a very important parameter that must be carefully controlled in order to determine the surface structure of the sapphire. The results show the machining width increase with the increase in energy fluence. Also, using a low scanning speed increases the pulses numbers in machining and it causes an increase in line width too.

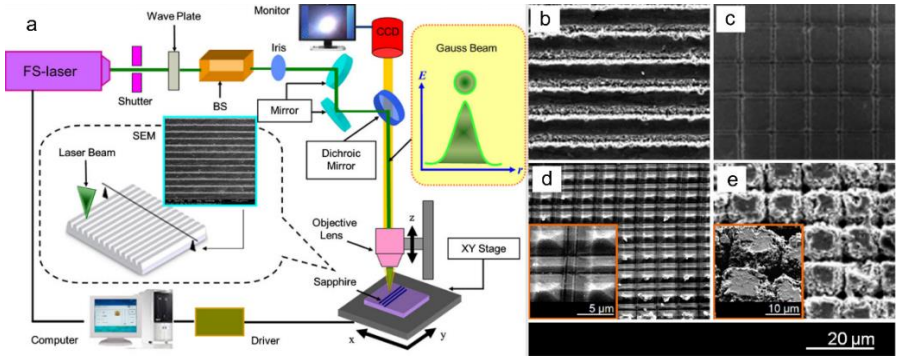

Figure 1-17. (a) Schematic of the experimental setup. (b) Gratings. (c) Square array. (d) Inclined groove-based array. (e) Square array [25].

To fabricate a high precision line without craters a low energy fluence and low scanning speed are needed. Since no linear absorption occurs in sapphire, the energy of the Yb FS laser (high peak power) can offer very short pulse durations that allow multiple photon absorption, i.e., nonlinear process. Due to the high energy fluence in the center of the laser, the center portion of the machined grooves has a greater depth. Figure 1-17 depicts a schematic of the experimental setup for surface structuring of sapphire and SEM images of four types of structures with different geometric sizes that could be machined on the sapphire surface [25].

Park et al used a low-power (continuous fiber-coupled diode laser) diode laser direct laser-assisted machining (SLAM) technique to improve the carbon-fiber-reinforced polymer (CFRP) machining process in comparison to the conventional machining method. They increased the target temperature with the laser to beyond the glass transition temperature to decrease the interfacial strength and improve the machinability of CFRP. The results showed a decrease in defects in cutting forces of both orientations (in-plane and side-cutting) and improved surface roughness when (DLAM) was applied. Additionally, a reduction in tangential force was obvious in DLAM, especially in cutting perpendicular to the fiber orientation in comparison to the conventional LAM method. The comparison of surface finish shows delamination and uneven breakage of fiber of in-plane cutting at conventional and a clean edge without fiber breakage in-plane cut with DLAM. Figure 1-18 shows schematics of the experimental setup and comparison of DLAM and conventional LAM machining method [26].

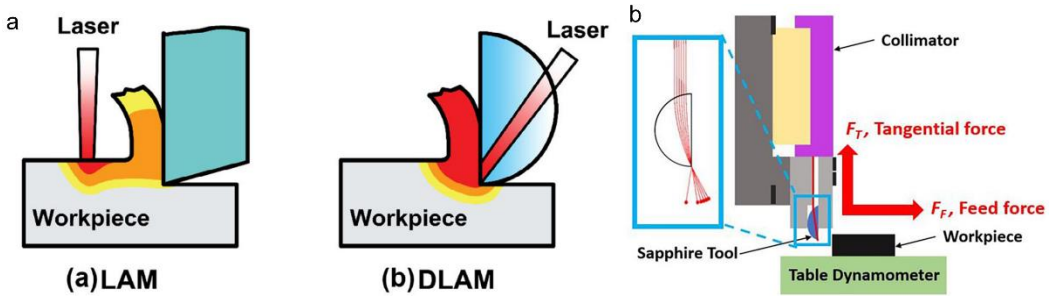

Figure 1-18. (a) Schematic of DLAM orthogonal cutting operation setup. (b) Conventional LAM and DLAM [26].

Cheng et al presented a laser direct-writing technology to develop a flexible platform for the rapid prototyping of glass microfluidic chips with a debris-free surface. A very low power high repetition rate UV laser was employed in laser-induced backside wet etching (LIBWE) for swift and affordable direct writing on glass. As shown in Figure 1-19, integrated surfaces with crack-free,

debris-free complex structures were easily generated by laser direct writing, which is very difficult with photolithography. As wet etching offers a complex process to fabricate structures with the same aspect ratio in multiple steps of photolithography, direct laser writing offers a simple, fast, and high-precision single micromachining process. Moreover, the direct-writing method can produce trenches with various aspect ratios by changing the laser parameters simultaneously on a single substrate [27].

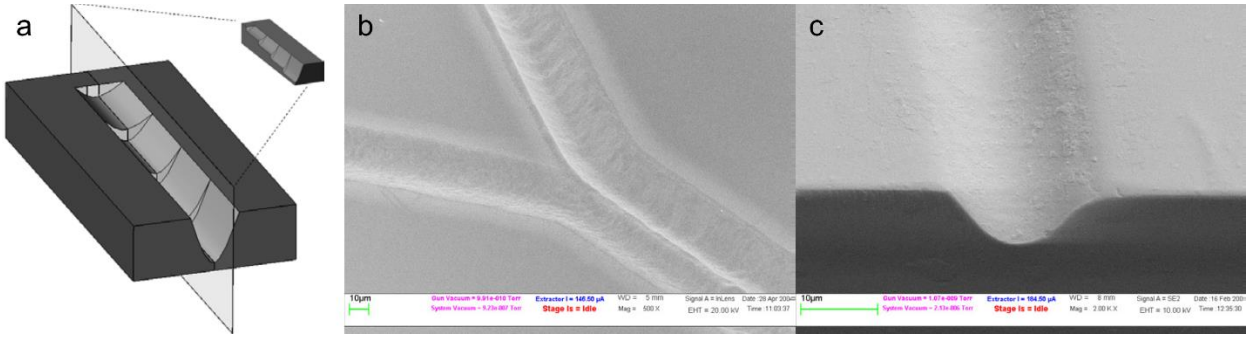

Figure 1-19. (a) Example of cut-view of the three-dimensional microstructure. (b) SEM image of two adjacent trenches that merge into an asymmetric trench. (c) SEM image of a 6 µm wide trench and 0.5 aspect ratio [27].

Bathe et al presented a laser surface texturing technique with different laser sources such as millisecond, nanosecond, and femtosecond laser which improves the tribological surface characteristics including load capacity, wear resistance, lubrication lifetime, and reduced friction coefficient. The effect of laser parameters such as laser pulse energy, pulse duration, and processing speed on surface laser texturing were investigated. Due to the high energy and longer pulse duration of millisecond laser-texturing, the surface partially melts and the bulges around dimples increase the surface roughness. Since the femtosecond laser has a shorter pulse-duration than milli- and nanosecond lasers, it left fewer resolidification and spatter particles, which caused the surface friction coefficient to be nearly 98% lower than the untextured samples. Figure 1-20 indicates the morphologies of the generated surface textures through different laser sources [28].

Mathew et al conducted a comparative investigation on surface quality and material removal rate between nanosecond and femtosecond lasers for on molybdenum plate. In micromachining with nanosecond laser micromachining, the machining width variation is directly proportional to the power. In the other words, the machining depth and width has direct relation with the laser power variation.

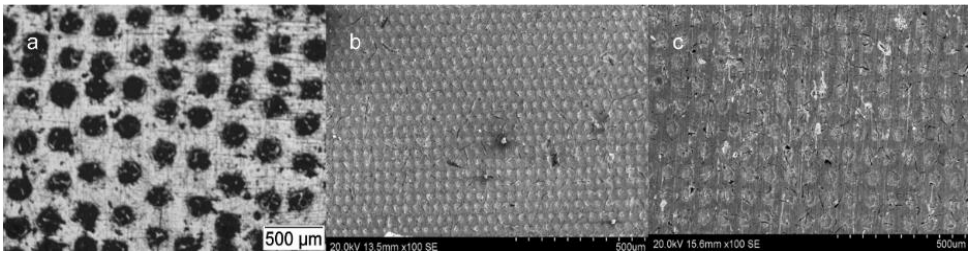

Figure 1-20. (a) Millisecond laser-textured surfaces. (b) Nanosecond laser-textured surfaces. (c) Femtosecond laser-textured surfaces [28].

The more the power, the more the material gets ablated but the heat-affected zone and recast layers increases at higher power. As the femtosecond laser has the shorter pulse duration than the nanosecond laser, laser pulses do not have enough time to create heat at the machining area, resulting decrease in HAZ and a high accurate micromachining generated. Figure 1-21 shows that the cutting quality of femtosecond laser is much higher than the nanosecond laser [29].

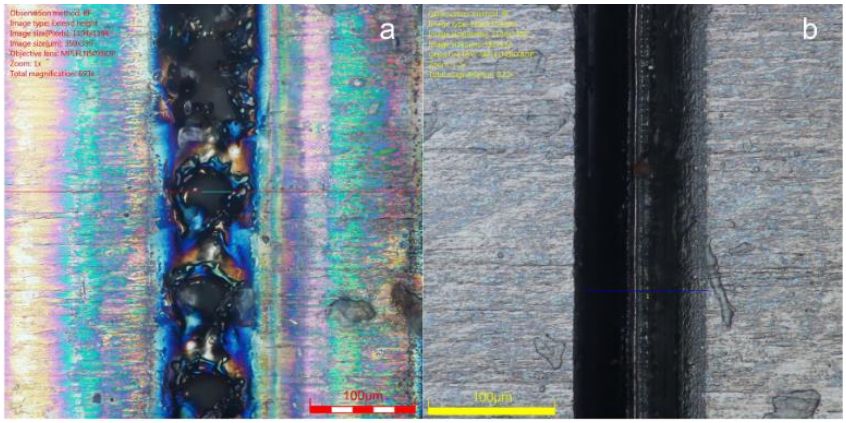

Figure 1-21. Optical images of machined grooves with: (a) nanosecond laser (b) femtosecond laser [29].

In this section, a brief review was carried out on laser micromachining methods such as different writing methods, ultrasonic-assisted, magnet-assisted, and laser-induced backside wet etching (LIBWE) by using different types of lasers such as pico/UV/nano/femtosecond laser. Based on the literature review, the advantages and disadvantages of each technique were identified. In addition, the effect of each type of laser on micromachining was identified. Since the nano/pico/femtosecond lasers produce short pulse duration and high peak power, they generate low heat affected zone, which provides highly accurate micromachining. In the next section, a brief review of different nanosecond laser micromachining techniques was caried out.

1.3 Nanosecond Laser Micromachining

A continuous wave or long-pulsed laser removes material by melting metal and ejecting it with an oxygen assisting jet. In Q-switched solid-state laser (nanosecond laser), ablation is the primary material removal mechanism, but melting of material still occurs during ablation of metals [30]. In the following section, different nanosecond laser micromachining investigation was reviewed.

Mandal et al. presented a low-power Nd: YVO4 laser micromachining of an aluminum alloy sheet. The effect of laser parameters such as laser power, pulse frequency, and scanning speed on machining width, HAZ, and surface roughness was investigated. They found that by increasing the laser power and frequency, the machining width and HAZ increases as well but increasing the machining speed reduces them. As the laser frequency increases, the interaction time between the surface and the heat is shorter which leads to less penetration of heat and more chances for heat to spread, resulting in greater machining width. Furthermore, if the laser power increases then surface roughness increases. On the other hand, by increasing in scanning speed the surface roughness decreases [31].

Xing et al developed the microchannels on a polycrystalline diamond (PCD) by nanosecond laser. Moreover, the effect of laser parameters such as power, frequency, and scanning speed on micromachining specifications were examined. They found that the laser power has a profound effect on the formation of micro-channels. Micromachining with low laser power reduced micromachining depth with a rougher surface. While, by increasing the laser power the material ablation increased, resulting in higher micromachining quality with fewer recast layers channels. Also, a decrease in scanning speed increases the interaction between the laser and the surface, resulting in increased material removal rate and more recast layers forming. Finally, they found that, micromachining with high laser power, low scanning speed and low frequency generates the greatest material removal but reduces the quality of machining due to recast layers [32].

Lin et al presented a micromachining approach on Mg-based Bulk metallic glasses (BMGs) using two kinds of nanosecond lasers including a 355 nm ultraviolet (UV) laser and a 1064 nm infrared (IR). Bulk metallic glasses (BMGs) are disordered materials that lack the periodicity of crystalline structures. The UV laser showed a higher and better micromachining and absorption rate than the IR laser. The cutting depth is depending on the laser parameters adjustment such as the laser power and scan speed. Figure 1-22 depicts the top and cross-section view of the laser machined area with

different laser sources. Due to the plastic deformation of machining area many materials re-deposited around the groove's edges. Plastic deformation is induced in the soft HAZ owing to the volume expansion of the irradiated region. Therefore, they could decrease this phenomenon by increasing the machining speed. Also, due to the lower rate of absorption by Mg-based BMG, the IR laser is not suitable for the micromachining process [33].

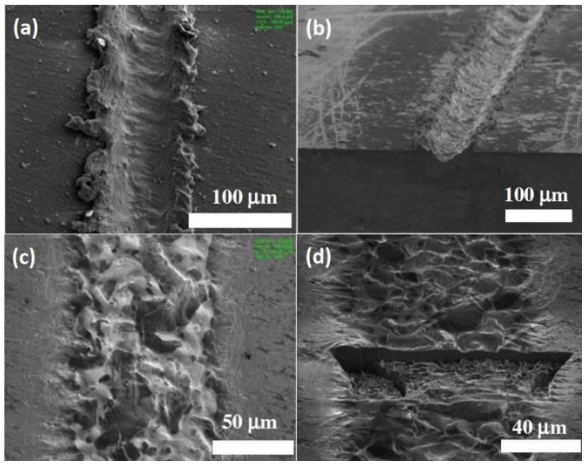

Figure 1-22. Top view and cross-sectional view of Mg-based BMG with (a) and (b) a UV laser micromachining. (c) and (d) an IR laser micromachining [33].

Kang et al presented an ultrasonic assisted nanosecond laser micromachining to improve the surface quality. The effect of ultrasonic vibration on surface was done through investigation of the morphological changes of particles re-deposited on the machined area. The applied ultrasonic vibration to the ns-laser micromachining improved the physical and chemical surface quality by preventing the surface oxidation and the formation of the recast layer. Since the ultrasonic assisted micromachining creates smaller and more uniform re-deposited nanoparticles in comparison of the conventional method, it left a better surface quality. This because the ultrasonic vibrations reduce the temperature which makes the floating nanoparticles less sticky. Figure 1-23 gives information about the concept of ultrasonic laser ablation process [34].

Teixidor et al studied the effect of near-infrared nanosecond Nd:YAG laser parameters on the geometry of microchannels fabricated from polymethylmethacrylate (PMMA) substrate. Since PMMA is a transparent with weak light absorption material, thus, a high fluence laser irradiation and low scanning speed is required for micromachining. The laser micromachining process parameters strongly affect the dimensional and geometrical quality of fabricated microchannels.

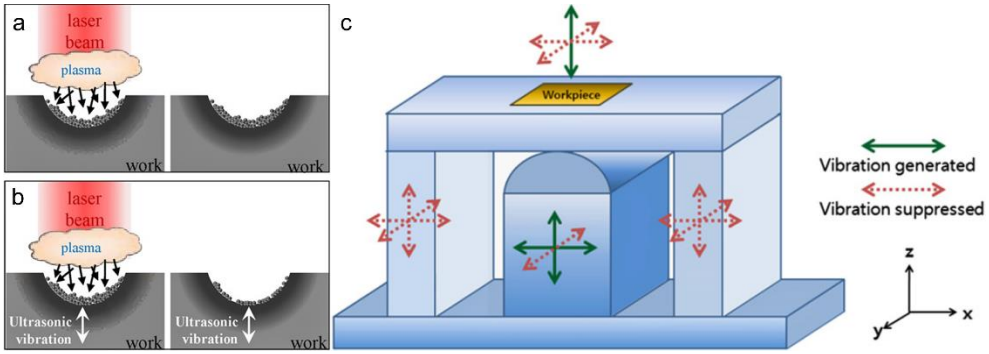

Figure 1-23. Concept of laser ablation processes by (a) Conventional method. (b) Ultrasonic-applied method. (c) Schematics of ultrasonic vibration module [34].

Due to photon energy attained to decompose molecular bonds in PMMA polymer and avoid cracking, Wavelength and fluence are more important than pulse duration and pulse frequency to obtain photochemical ablation. Figure 1-24 indicates the experimental setup for the laser micromachining of microfluidic channels on (PMMA) substrate [35].

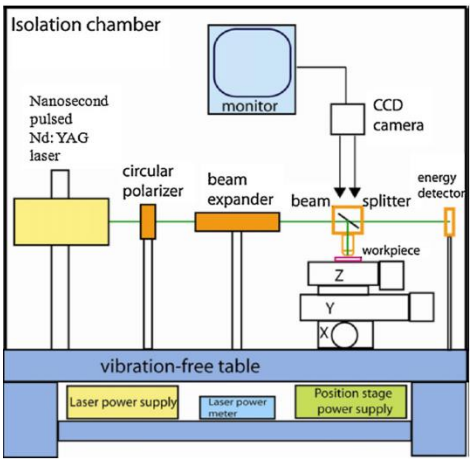

Figure 1-24. The experimental setup for the laser micromachining of microfluidic channels [35].

Tangwarodomnukun et al showed a novel laser micromachining on silicon in a thin layer of ice reduce the excessive heat and prevent cut debris deposition. Figure 1-25 shows a comparison between the microgrooves from the laser ablation of silicon in ambient air and ice. The excessive heat generation can have a negative impact on micromachining roughness and cleanness which is decreased with ice assist. On the other hand, it causes the machining depth to be greatly reduces. This phenomenon can be justified in two ways. First, the cooling effect of ice may strongly impact the laser heating and decrease the heat energy. Second, the ice layer can decrease the laser energy absorption into the workpiece surface [36].

Figure 1-25. Cross-section and top views of microgrooves: (a) air (b) -10° ice. (c) Schematic of laser micromachining process under an ice layer [36].

Behera et al used a nanosecond-pulsed laser to study the input parameters to fabricate high-quality microchannels on 304 stainless steel substrates. Increasing the laser scanning speed, decreases the interaction time between material and laser pulses resulting in fewer material removal rates but leads to less formation of the recast layer and debris. Due to the high thermal conductivity of the material, kerf width sharply rises with an increase in the scanning pass number. Furthermore, the microchannels depth variation is proportional to scanning passing number. Increasing in the scanning passing number rises the laser beam penetration and increase the depth and surface roughness [37].

As we used a nanosecond laser in our study, a brief review based on different nanosecond laser micromachining techniques such as direct writing, ultrasonic-assisted, and ice-assisted was carried out. Based on the literature review, the advantages and disadvantages of this laser micromachining were identified. In nanosecond lasers, material removal occurs through ablation. While the aforementioned review primarily focused on surface micromachining in 2D, different techniques in 3D laser micromachining shall be reviewed in the next section.

1.4 3D Micromachining

Most microfabrication processes are developed for 2D fabrication and cannot build complete 3D microstructures. To optimize the fabrication of structures on the scale of micro and nano, 3D micromachining systems must be developed. As mentioned earlier, the laser micromachining technique structure is based on material removal via ablation. Due to its high precision machining, reliability, and fewer manufacturing steps, laser micromachining attracted a lot of attention in the industry for generating 3D microstructures [38]. Therefore, a brief criticism of different 3D laser micromachining methods by using various laser types was conducted.

Liu et al designed an ultraviolet nanosecond pulse laser micro-fabrication system for the fabrication of 3D microstructures on a single-crystal silicon wafer, plexiglass, and ceramic tube

substrates. A Z-directional step motor stage was used to move the sample to the focus. Moreover, a computer-controlled the 3D direction movement of the system to support the graphics. Given those different materials exhibit different behavior, the laser parameters were varied for each experiment. Since the high scanning speed generates discontinuous spots on the sample, micromachining with high laser power and low scanning speed was suggested to achieve uniform deep micromachining. As plexiglass is a transparent material, the 355 nm ultraviolet pulse laser cannot be absorbed well by plexiglass and left a discontinuous line. Therefore, they found that choosing a suitable target is very important for high-quality micromachining. Since the ceramic showed a good response to the laser ablation, two holes were fabricated through laser drilling. Figure 1-26 depicts the fabricated graphic on the single-crystal and ceramic substrates [39].

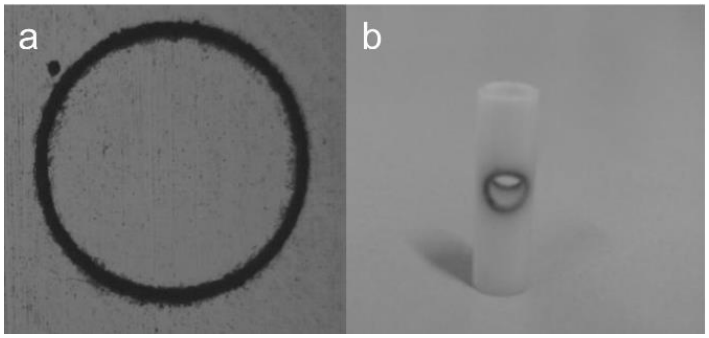

Figure 1-26. Graphics fabricated by the system on the: (a) single-crystal (b) ceramic tube [39].

Huang et al presented the fabrication of a through-wafer microfluidic structure in a bulk silicon carbide (SiC) by an ultrafast femtosecond pulsed laser. The laser parameters as well the surface wettability of the laser-affected surface was examined. They found that since the thermal penetration of femtosecond laser is low, the width ablation is faster than the depth. Furthermore, mineral oil flowed into the microfluidic channels to measure the contact angle of the machined surfaces. The results show that the wettability of the surface improved with an increase in surface roughness through laser ablation. Additionally, femtosecond laser showed high flexibility in creating microchannels of various cross-sectional shapes. Figure 1-27 shows a schematic of the femtosecond micromachining system [40].

Kam et al used a Q-switched Nd:YAG laser to fabricate a multi-depth and multi-width microchannel network with a 3D tapered inlet connection on a silicon substrate. The argon gas was injected at a 45° angle to eject the molten material from the microchannels and increase the

ablation rate. In addition, wet chemical etching was used to remove debris buildup caused by micromachining.

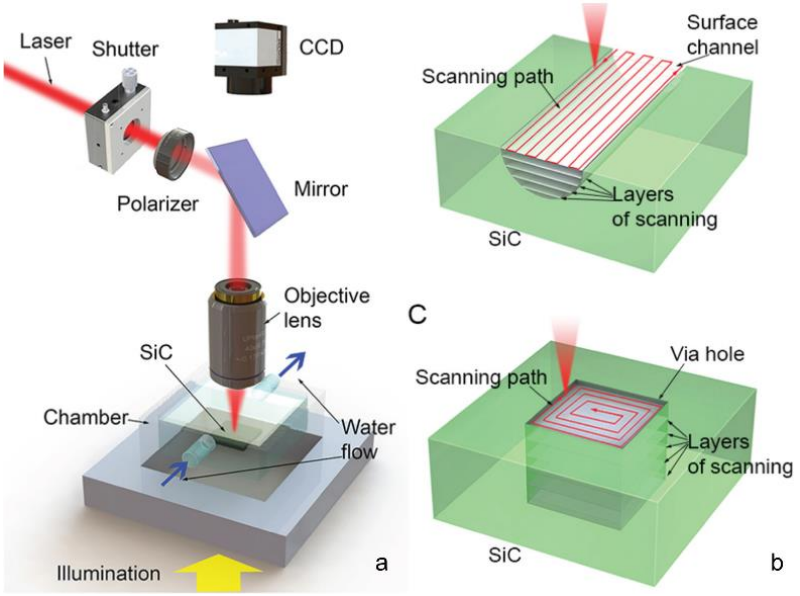

Figure 1-27. Schematic of the femtosecond laser micromachining system. (A) Optical setup. (B) Channel laser scanning. (C) Hole laser scanning [40].

The argon gas injection assist was significant in the ejection of the molten materials from the channels and generating a uniform surface. The key to fabricating multi-depth and multi-width channels was to alter the number of laser beam passes. Figure 1-28 illustrates the SEM images of laser machined microchannels with and without gas injection [41].

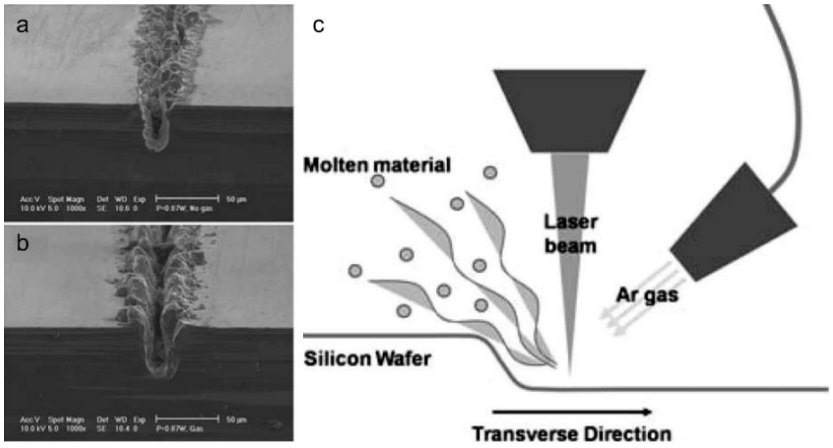

Figure 1-28. The SEM images of laser machined microchannels: (a) without gas injection and (b) with argon gas injection. (c) Schematic sketch to illustrate the role of argon gas injection [41].

The micro electrical discharge machining (micro EDM) is high precision micromachining that has a slow machining speed and high tool wear, and nanosecond pulsed laser micromachining is a fast and non-wear machining process. Kim et al introduced a hybrid micromachining technique by combining two methods of micro EDM method and laser ablation micromachining to reduce the disadvantages of each method and fabricate the high precision 3D microstructures such as drilling and milling. First a laser micromachining was performed to create a micro-hole which left a large amount of the recast layer around the hole entrance. Then, a post-drilling process was performed through the micro EDM to remove the recast layers. This hybrid micromachining technique improved the micromachining efficiency, accelerated the process, and reduced the tool wear by 12%. Figure 1-29 gives information about the concept of hybrid micromachining and the result.

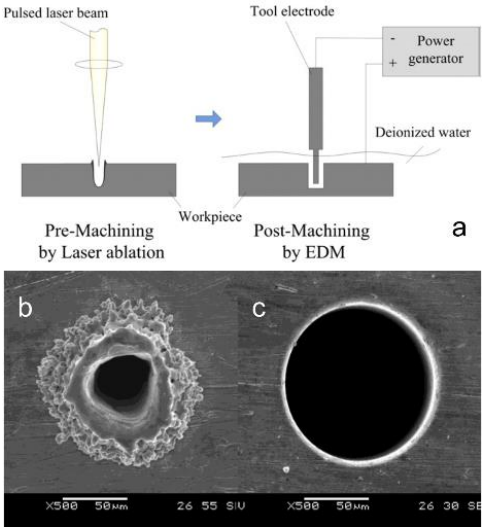

Figure 1-29. (a) Concept of hybrid micromachining. (b) SEM image of laser ablation. (c) SEM image of hybrid process [42].

In milling process, a repetitive rough laser micromachining along a linear route at a constant scan speed was done to create a groove. A high laser power and fewer pulse repetition rate was suggested to generate a U-shaped groove which makes it easier to achieve vertical walls and improve the machining efficiency. Then, same as micro-drilling a post-drilling process was performed to remove the recast layers. This hybrid milling process enabled production of different 3D microstructures with various depths and shapes. Figure 1-30 indicates some micro-millings which are generated through hybrid micromachining system [42].

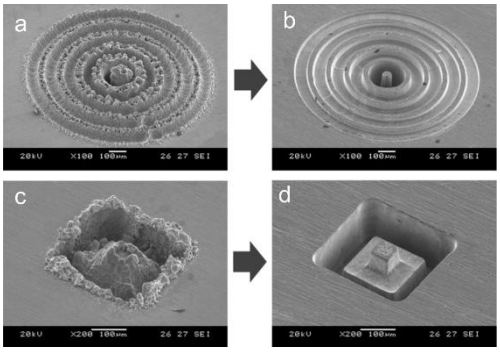

Figure 1-30. Microstructures fabricated by the hybrid process: figures on the left ((a) and (c)) are after laser pre-machining and figures on the right ((b) and (d)) are after the hybrid process [42].

Knowles et al used the nano/picosecond laser to generate 2.5D microstructures in alumina, tungsten, and steel substrates. Both lasers presented an excellent performance in surface micromachining with high material removal rate. As there is no evidence of melting in ceramics, micro-milling with short pulse and wavelength left a high-resolution microstructure with no cracking or other collateral damage. In addition, since dielectrics such as fused silica is transparent at 511nm, laser micromachining of them by nanosecond copper vapor laser (CVL) is not possible. Therefore, by repeated passes of 1064 nm Ps-laser beam over the exposed area made the 3D micro-milling possible without evidence of microcracking or other collateral damage. The direct writing capability of laser micromachining made it a very flexible method to create a component by using drilling, cutting, and milling in a single operation. Figure 1-31 shows the laser milling of Alumina and fused silica through 1064 nm picosecond laser [43].

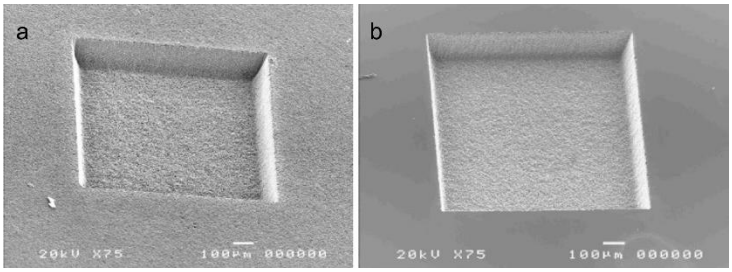

Figure 1-31. Picosecond laser (1064nm) milling of (a) alumina, and (b) fused silica [43].

Liu et al presented a new nanosecond pulsed laser micromachining system to fabricate the 3D micro-features on the silicon substrate. Mechanical (3D platform) and optical structures are designed for laser beam focusing. The result of the parameter experiments shows that a desirable depth and width can be achieved by optimizing the parameters. It was obvious the movement of

the work platform, low machining speed, and high laser power can affect the micromachining to achieve deeper and wider grooves. Moreover, they found that some micromachining optimization and assists such as processing repeatedly with low energy instead of single processing, blowing air while processing, cleaning the surface with alcohol after processing, etc., can help to fabricate accurate and clean microstructures with a low aspect ratio [44].

Heyl et al designed a high-precision UV light laser ablation system to generate 3D microstructures on hard metals and dielectric materials such as ceramics, diamonds, polyimide, and PVC. To avoid strong melt rejections, the initial focus diameter was increased. Therefore, due to plasma formation, the laser absorption will decrease. The laser ablation method has a higher speed and geometrical flexibility which leads to equivalent surface quality when compared with the traditional high-end electrical discharge milling (EDM) procedures. Furthermore, they found that the higher ablation per pulse generates a steeper wall. Figure 1-32 depicts a schematic of laser micromachining system and S.E.M.-pictures of example geometry [45].

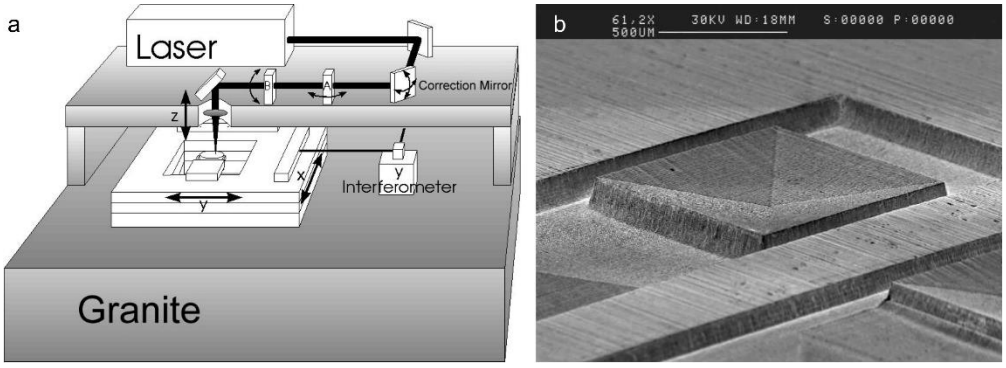

Figure 1-32. (a) LAM schematic design. (b) S.E.M.-pictures of example geometry [45].

Žemaitis et al introduced two methods to study the dependency of laser efficiency to the parameters and scanned line distance for the copper sample. A picosecond laser and a galvanometer scanner were considered to do a layer-by-layer removing technique with optimal parameters to fabricate the 3D features. For the first method, the beam spot size was kept constant and the other laser parameters were varied. In order to achieve the highest ablation efficiency, the laser power should be limited to avoid getting a linear dependence on ablation rates. In the second method, the laser power was kept constant, and the beam spot size was enlarged until it reaches the optimum fluence point. The optimum fluence point depended on beam scanning speed and pulse repetition rate. By increasing the laser fluence the roughness of the bottoms of the cavities increased steadily. This is

due to the waste energies which could not remove the materials and deteriorate the surface quality. By scanning with higher speed decreased the material melting, redepositing did not occur, and a better morphology was observed. The laser beam shifted down to replace it at the focal point to remove the unwanted materials to generate a fast 3D fabrication. The combination of a rotary axis with the galvanometric scanner made the 3D objects fabrications possible. Figure 1-33 shows a schematic of machining process and SEM images of laser microstructure [46].

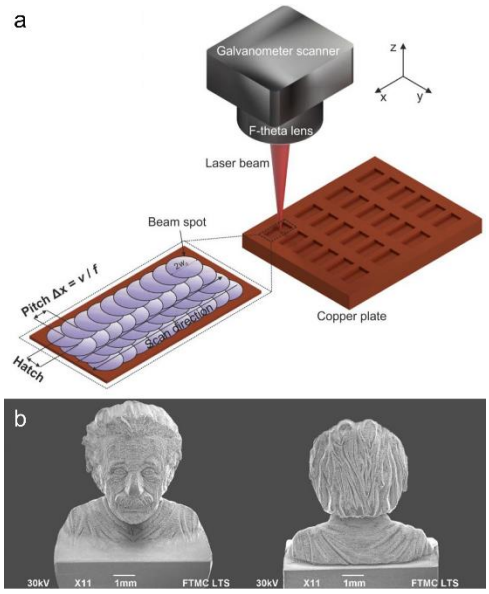

Figure 1-33. (a) A simplified view of copper plate processing, which shows the beam scanning trajectory, beam spot width, hatch, and pitch distances. (b) SEM images of both-sided laser sculptured bust [46].

Wang et al presented an immersion waterjet assisted laser micromachining (IWALM) method to flush out the removed materials, plasma, and micro bubbles away from the scanning target and minimize the HAZ, recast layer, and the taper angle around the entrance of machining area. It was found that IWALM micromachining produced better quality and efficiency than micromachining in the air. Moreover, the results indicated that a higher waterjet flow speed and a smaller nozzle-workpiece gap improve the machined surface quality. In this way that, flushing the bubbles from the machining area reduces laser beam reflections and scattering, increasing machining depth and quality. Further, it was observed that with increasing laser intensity, the taper angle decreased, and processing efficiency was improved. Figure 1-34 indicates a schematic of developed experimental setup [47].

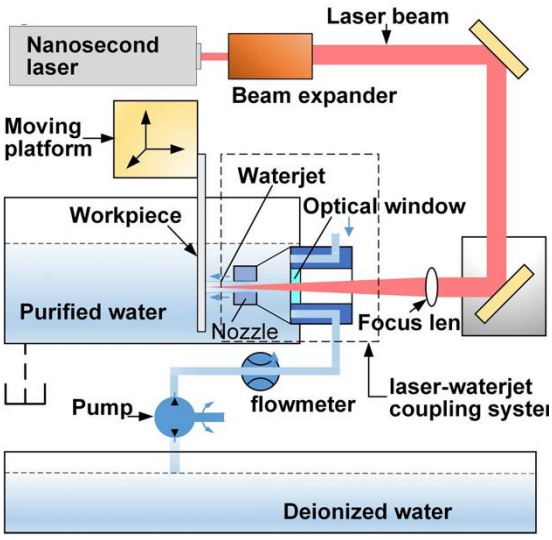

Figure 1-34. Schematic of developed experimental setup for IWALM [47].

Fang et al combined nanosecond laser and two-axis reflection control to fabricate a 3D pyramid-like patterns on cemented carbide substrate. They found that a better contour could be defined by increasing the number of sides and slope angles. Furthermore, when the side angle increases, polygon sides become more straight and molten material get clean easier, in result machining quality improves. Since a brittle layer-by-layer structure forms during the cooling process of molten materials, a smaller laser fluence was suggested for fabrication of more sophisticated profiles. On the other hand, as the reduction in laser fluence increase the machining process longer, pico/femtosecond lasers were suggested instead of nanosecond laser to avoid the thermal reaction. Figure 1-35 Illustrates the composition of setup and laser beam path [48].

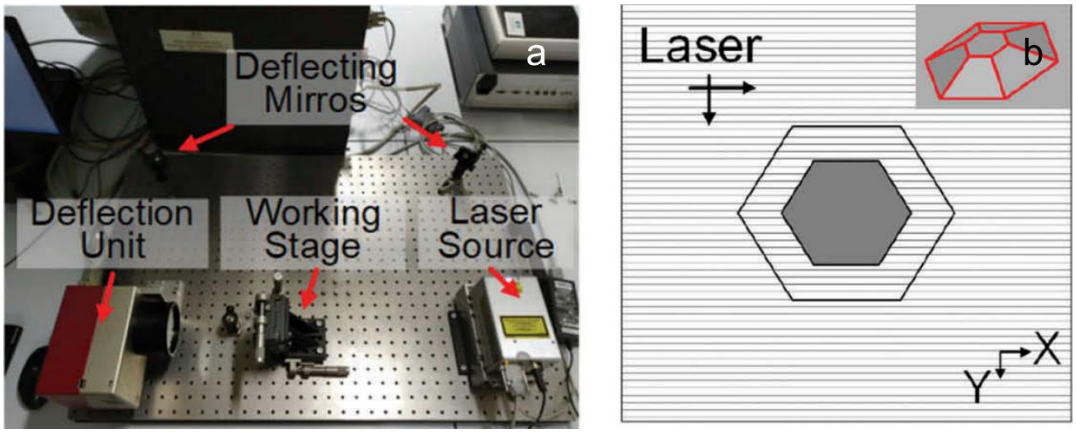

Figure 1-35(a) Schematic illustration of the laser machining parameters. (b) Laser beam path [48].

Sugioka et al presented a direct femtosecond (fs) laser micromachining to form 3D hollow microstructures embedded in photosensitive glass through multiple absorption, thermal treatment, and successive chemical wet etching in a hydrofluoric (HF) acid (Figure 1-36).

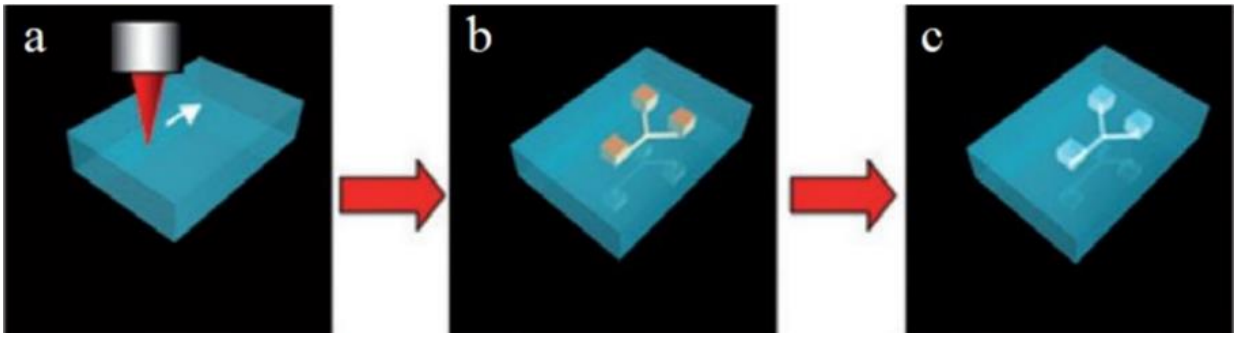

Figure 1-36. Schematic of the fabrication procedure of 3D hollow microstructures inside the photosensitive glass. (a) Fs-laser direct writing. (b) Heat treatment. (c) Etching [49].

Since the air has a lower refractive index than the glass, a hollow microplate was embedded into the glass chip to generate a 45° internal micromirror. A He-Ne laser beam was irradiated into the glass to check the optical characteristics of the produced three-dimensional micromirrors. Furthermore, one of the inner sidewalls of the structure is spherical and can act as a plano-convex lens, enabling the fabrication of micro-optical lenses within the glass chip. A computer controlled XYZ stage was considered to move the sample perpendicular to the laser beam axis.

To produce biphotonic microchips, first, the latent image of the microlens is written with direct laser writing, followed by the latent image of the microchamber directly next to it. After heat treatment, a wet etching was performed to fabricate two micro-components such as microfluidic chamber and the micro lenses. After wet-chemical etching, the etched surface is significantly smoothed by additional heat treatment, which leads to the use of this process to produce micro-optical elements inside photosensitive glass.

By adding heat after wet etching, the etched surface is smoothed greatly, leading to the use of this process for producing micro-optical elements in photosensitive glass. Figure 1-37 depicts schematic configuration of 3D integration of two waveguides with a micromirror and an optical planoconvex microlens [49].

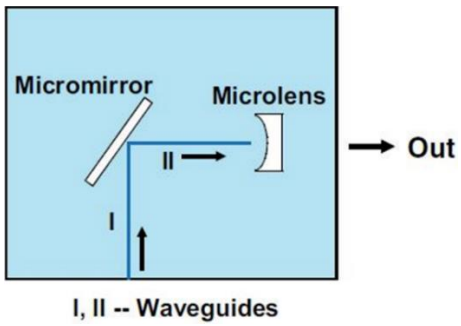

Figure 1-37. Schematic configuration of 3D integration of two waveguides with a micromirror and an optical planoconvex microlens in a single glass chip [49].

In this section, an overview of different direct writing, assisted, and hybrid 3D laser micromachining techniques were conducted. Based on the literature review, it revealed that laser parameters have a significant effect on 3D micromachining. Furthermore, micromachining assistance like adding gas, ultrasound, etc., can improve the machining quality. In addition, hybrid systems like EDM and etching can enhance the surface quality of microstructures.

1.5 Motivation

With the comprehensive study of laser micromachining and 3D laser micromachining, it is observed that there is not a thorough investigation on laser micromachining parameters to achieve 3D microstructures. Moreover, 3D laser micromachining requires an assisting approach to push or wash out the debris resulted by machining. As of today, the methods presented are not affordable easy to implement and accessible. Furthermore, there is no fast and low-cost laser micromachining system that all optical components work simultaneously to generate a 3D microstructure in a single scanning process. This gives a motivation to develop a 3D laser micromachining assisted by air jet system, which can provide a high-precision, fast, and single-process 2D & 3D micromachining. Therefore, an attempt was made to develop a 3D laser micromachining setup, in the Laser Metrology and Micromachining Laboratory (LMML) of Concordia University, where significant amount of research is being performed in the field of peening using a high repetition rate and low energy laser.

1.6 Objective

Primary goal of this thesis is to develop a 3D laser micromachining setup for the purpose of micro-molding. To accomplish the objective, the scope of this research work would include:

Optimization of 2D laser micromachining conditions

- To investigate the effect of opto-mechanical parameters including laser power, pulse overlap and number of pulses in a spot on the depth of machining and the surface roughness.
- To develop an algorithm for extracting the machining coordinates from the image of pattern
- To study the accuracy of the 2D laser micromachining setup in fabrication of complex shapes

Development of 3D laser micromachining

- To develop an experimental setup for 3D laser micromachining assisted by air-jet and using a stage to achieve samples movement along the laser irradiation direction
- Analyzing the effect of the laser power on the 3D laser micromachining
- Validation of 3D laser micromachining approach presented in this work by making 3D complex structures
- To present the proof of concept in using the 3D micromachined structure as a mold for microfabrication of PDMS parts

1.7 Organization of the thesis

This thesis consists of five chapters. In the first chapter, a literature review on non-laser-based micromachining, laser-based micromachining, and 3D laser micromachining is overviewed. Based on the literature review, the research problem was identified, and the objectives for developing a laser micromachining system for purpose of 2D & 3D micromachining were identified.

The second chapter deals with the materials (optical components) used for laser micromachinings with their technical details, the number of tests, design of the experiments, development of MATLAB algorithms, and measurement devices are described.

In the third chapter, an evaluation of the laser parameters such as overlap, laser power, and the number of pulses were conducted in terms of machining depth, surface roughness, and machining quality. Furthermore, a 2D micromachining of a complex shape was conducted to evaluate the accuracy of the laser micromachining system.

The fourth chapter gives an overview of the 3D laser micromachining feasibility and micro-molding. A laser micromachining experiment was designed to evaluate the feasibility of 3D micromachining. Then, a 3D laser micromachining was conducted to evaluate the machining accuracy in the fabrication of 3D complex microstructures. Finally, the 3D microstructures were molded to fabricate the PDMS structures. In addition, in the fifth chapter, the conclusion and future works are presented.

1.8 Contribution from the thesis

- Shayan Mohammadi Pour Khajani, Hamid Ebrahimi Orimi, Sivakumar Narayanswamy, "Investigation of the impact of opto-mechanical parameters towards high-speed manufacturing of 3-dimensional patterns with nanosecond laser" Photonic North, 2020, Niagara Falls
- Shayan Mohammadi Pour Khajani, Hamid Ebrahimi Orimi, Sivakumar Narayanswamy, "Nanosecond laser 3D micro-molding" In preparation to be submitted to journal of manufacturing

CHAPTER 2. MATERIALS AND METHODS

In this chapter, first different mechanical features of the setup are presented. The material properties of the specimen, methods and techniques used for conducting the experiment are discussed. Lastly, description of result and the analysis are stated in detail.

2.1 Laser

The laser model that was used in the current research for micromachining purpose is Coherent MATRIX 532-14-40 (Figure 2-1). The laser is a Nd:YVO_4 Diode Pumped Solid-State (DPSS) laser. This is a pulsed solid-state Q-switched laser having a wavelength of 532 nm and a pulse duration of <20 ns. The repetition rate of the lasers pulses can be tuned from 10 kHz to 200 kHz. The maximum power is 14 W at 40 kHz repetition rate. The laser power can be varied to lower than 14 W by changing the input voltage.

Figure 2-1. Coherent MATRIX 532-14-40 [https://www.coherent.com/]

2.2 Opto-Mechanical Components

A galvanometer, converging lens, mirror, and an adjustable stage/fixture to hold the samples are all essential optical components in this laser micromachining setup. Due to the parallelism and correct size of the laser beam, there is no need for a telescopic lens. The optical setup is calibrated so that the laser beam reaches the galvanometer and then is directed to the center of the converging lens to achieve the maximum scanning range. Then, after passing the laser beam through the converging lens, it reaches a 45° mirror so that we can direct the beam towards the sample to make the micromachining possible.

It is crucial to be considered that all the optics should be at the same height and well-aligned. Figure 2-2 shows the laser micromachining setup.

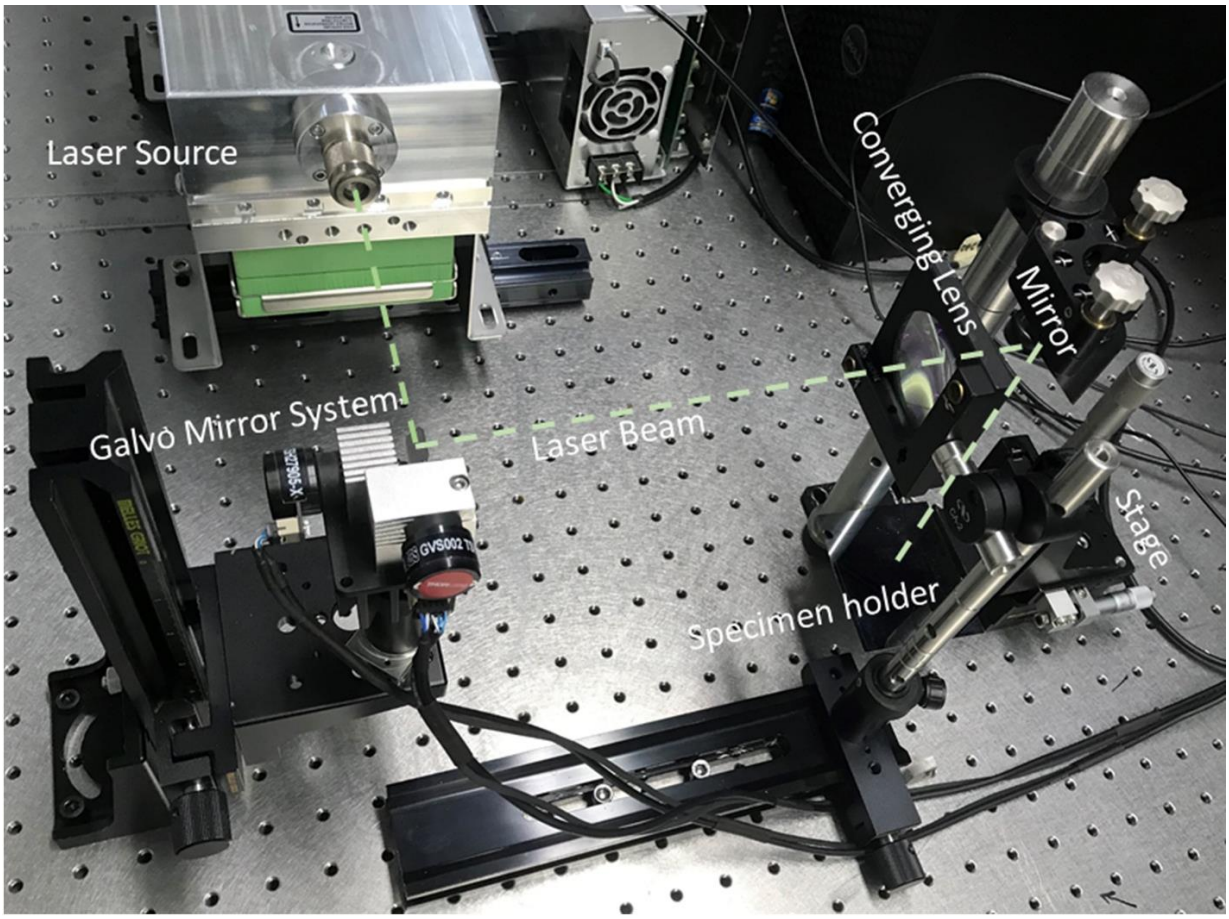

Figure 2-2 Laser micromachining experimental setup and opto-mechanical elements

A high-speed scanning galvoscanner (THORLABS GVS002) was used to control the movement, scanning speed, size, and location of the laser beam on the specimen. This system is consisting of two silver-coated mirrors which are controlled by two servo DC motors separately. The servomotors are controlled with a NI 6211 USB DAQ card. The angular rotation of the mirrors depends on the input analog voltage. In other words, the rotation angle of the mirrors can be controlled by changing the input voltage. The range of the analog voltage is between -10 to 10 V and the corresponding range of motion of each motor is between -12^{o} to 12^{o} which provides motions at a resolution of 1.2°/V. Figure 2-3 illustrates a schematic view of how galvo mirrors and entire optics work.

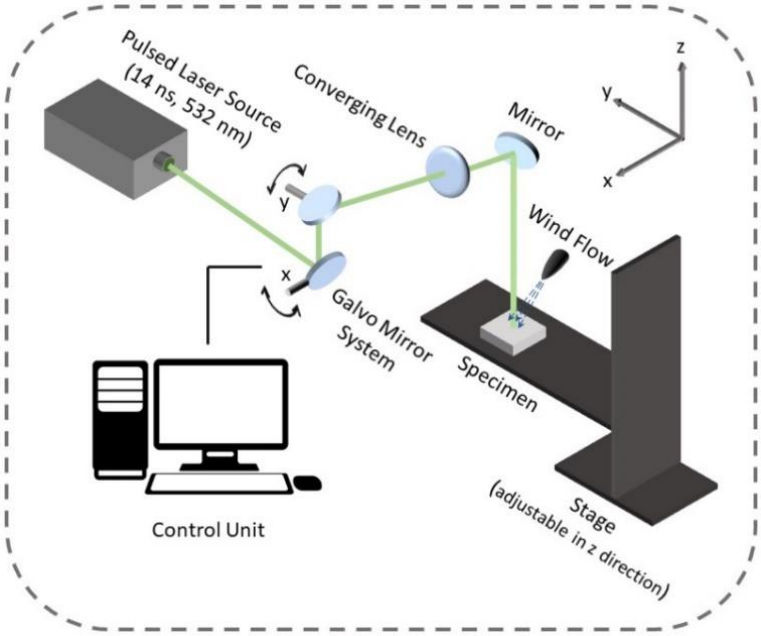

Figure 2-3. Schematic of the 3D Laser Machining Setup

The laser beam perpendicularly hits the converging lens with a diameter of 50 mm that has been placed 200 mm (at the focal plane of the lens) away from the galvanometer mirrors. The magnesium sample was fixed at 200 mm away from the lens on the stage at the focal point. Due to the position of the sample in the setup, a 45° mirror was placed between the lens and the sample to guide the laser beam perpendicular to the sample for the laser micromachining.

2.3 Equations

The diameter of the emitted laser beam from the laser source is fixed and it is 0.23 mm. The minimum possible beam spot size can be calculated by Eq. (2.1).

$$d = 1.27\, f\lambda / D \qquad \text{Eq. (2.1)}$$

Where 'd' is the spot size, 'f' is the lens focal length which is 200 mm, 'λ' is the laser wavelength which is 532 nm and it is a constant parameter, and 'D' is the initial laser beam diameter which is 0.23 mm. By using the Eq. (2.1), the spot size was calculated, and it was 58.7 µm. It is clear that by decreasing the focal length, the spot size will get smaller. On the other hand, to reduce the focal point, the lens should be placed at a closer distance to the galvo mirrors, which results in the reduction of scanning range, and it impacts the focusing due the back focal length. Therefore, the spot size of 58.7 µm was considered as the least possible spot size 'd' for this optics.

As overlap is one of the variable parameters in this work, we need to find a scanning speed that can provide a certain overlap percentage. Scanning speed is calculated using Eq. (2.2) and Eq. (2.3) calculates the pulse pitch.

$$Scanning\ speed\ (\mu m/s) = Pulse\ pitch \times Pulse\ repetition\ rate\ of\ the\ laser \quad \text{Eq. (2.2)}$$

$$Ov = d \times (1 - Op) \quad \text{Eq. (2.3)}$$

Where the Ov is the pulse pitch, d is the spot diameter of the laser and Op is the percentage overlap. For example, for a 0% overlap the pulse pitch is calculated from Eq. (2.3) to be 58.7 µm.

$$Ov = 58.7 \times (1 - 0) = 58.7$$

The overlap in the x-direction is controlled by the pulse pitch and by the speed of the y-axis mirror by using Eq. (2.2) and Eq. (2.3). Figure 2-4 is the schematic of spots for 0%, 40%, and 80% overlap.

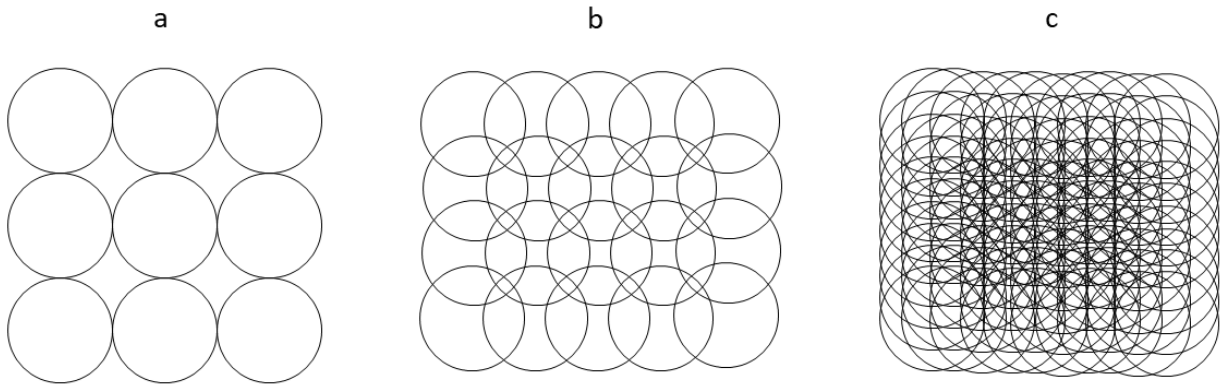

Figure 2-4. Schematic of the samples textured under three different overlap values, (a) 0%; (b) 40%; and (c) 80%.

$$Ov = 2f.tan\varphi \quad \text{Eq. (2.4)}$$

In Eq. (2.4), f is the distance between the galvoscanner and the converging lens, and φ is the rotation angle of the galvomirrors. From Eq. (2.4), $\varphi = Arctan(Ov/2f)$ where $f = 2 \times 10^5 \mu m$, therefore, $\varphi = Arctan(Ov/4 \times 10^5)$.

$$\varphi = Arctan(58.7/4 \times 10^5) = 8.4 \times 10^{-3^\circ} \text{ and } voltage = 7 \times 10^{-3}\ V \quad \text{Eq. (2.5)}$$

Accordingly, to obtain a textured pattern with 0% overlap, the corresponding value of the pulse pitch is 7×10^{-3} volt. From this proportionality, we can find that:

$1\mu m \sim 0.12 \times 10^{-3}\ volt.$

And the scanning speed for 0% overlap at repetition rate of 20 kHz can be calculated from Eq. (2.2) as 58.7 µm×20000=11.7×10^5 µm/s.

A MATLAB algorithm was developed to control the galvomirror's motors angle to guide the laser beam to the machining area in desired coordinates. Based on the machining area the maximum and minimum analog input voltages are calculated, and Eq. (2.6) shows the relation between the maximum displacement and the DC motor angle.

$$\alpha = tan^{-1}(\frac{x}{f}), \beta = tan^{-1}(\frac{y}{f}) \quad \text{Eq. (2.6)}$$

Where α and β are the rotation angles of the galvomirrors in the x and y directions respectively; x and y are the coordinates in x and y directions and f is the focal length of the lens. It is important to note that the distance between the galvoscanner and the lens was also defined as f earlier. If and only if the distance between the galvoscanner and the mirror same as the focal length the scanned laser beam will impinge normal to the workpiece.

Another variable in this work is the number of pulses per spot. This is controlled by placing the laser beam on the specific coordinates for predetermined dwell time. For this purpose, sending command is delayed by the DAQ card. Since the laser runs by 20 kHz repetition rate, to have 50, 100, 200, 400 and 4000 pulses per spot, the delays between commands are 2.5, 5, 10, 20 and 200 ms, respectively.

2.4 Controlling Software

MATLAB algorithms have been developed to control the movement of the galvoscanner mirrors. As mentioned earlier each galvo mirror was attached to a servo DC motor and the motor was controlled with a NI6211 USB DAQ board. For machining a shape, first, the shape was created as a picture file or any available image files can be used. The image was then uploaded into MATLAB and scaled to the required micromachining size. Then, the captured images were processed by

MATLAB, and converted to a binary image. Knowing the percentage of overlap, the address and distances between each spot were calculated and converted to coordinates. Finally, the laser beam was guided to the desired coordinate by moving the galvanometer mirrors. Figure 2-5 shows the schematic representation of the developed algorithm.

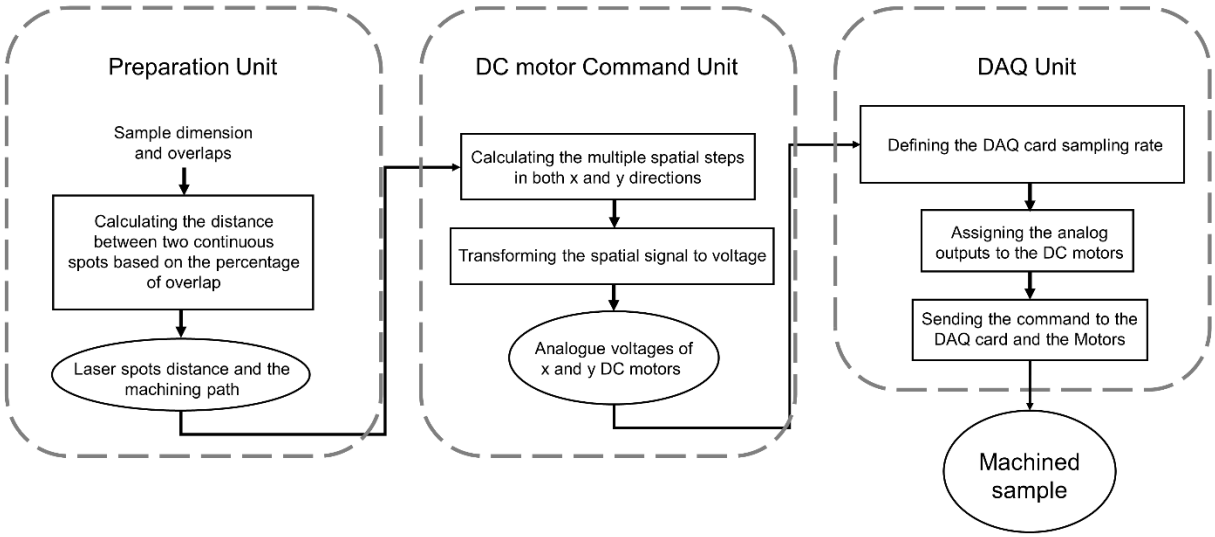

Figure 2-5. Schematic of the developed algorithm for curved shapes.

2.5 Magnesium

Recently, Magnesium (Mg) finds enormous application in construction and industry that can be replaced with denser materials due to its light weight. Apart from being a light alloy, it has other advantages that encouraged us to use magnesium in this study, including the lowest density of all metallic constructional materials, high specific strength, good castability, much-improved corrosion resistance using high purity magnesium, and it is readily available [50]. The magnesium rod with a diameter of 33 mm was cut by a saw to 5 mm-thick layers. Then, the cut layers grinded to achieve a soft surface for micromachining. Finally, the grinded magnesium layers were cut to 10 mm×10 mm pieces for laser micromachining experiments (Figure 2-6).

2.6 Air Jet

When the laser beam removes the material from the sample, some of the ablated materials turn into debris in the machining area. In such a way that the ablated material stays in the machining

zone and will leave sediment in the area which prevents the laser beam to reach the bottom of the grooves. This phenomenon reduces the micromachining depth and accuracy and increases the surface roughness.

Figure 2-6. Magnesium (Mg) sample [50].

In order to reduce the impact of this phenomenon, airflow was directed during the laser micromachining to eject the produced debris much easier and faster from the micromachining area. First, the specimen was fixed on the stage to prevent it from moving during the applying air jet. Then, three-bar air jet was applied into the micromachining area simultaneously with the laser micromachining.

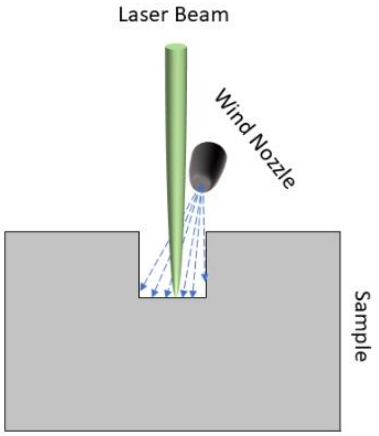

Figure 2-7. Schematic of applying air jet on micromachining area

The air jet is supplied by the common pressurized output in the lab which can cover pressure range of 1-11 bar. This technique has a noticeable effect on the surface roughness reduction and increases the surface quality of the fabricated features. This manufacturing improvement was remarkably effective in 3D micromachining. Figure 2-7 shows a schematic of this technique.

2.7 Confocal Microscopy

The LEXT OLS4000 3D Laser Measuring Microscope presented in Figure 2-8 was used for the measurements of roughness, morphology, and depth of 2D and 3D profiles (Concordia University Logo and the pyramid). This model provides excellent imaging quality and accurate 3D measurement with advanced optical system. Confocal microscopy uses laser light to excite a specimen within a narrow plane of focus. Confocal microscopy produces sharp images of the exact plane of focus without interference of fluorescent light from the background. LEXT OLS4000 can measure acute-angled specimens, which were previously impossible. The magnification range of this model is between 108x and 17,280x.

Figure 2-8. LEXT OLS4000 3D Laser Measuring Microscope [https://www.olympus-ims.com/en/].

2.8 White Light Interferometer

WYKO NT1100 interferometer presented in Figure 2-9 was used to determine the surface profile and morphology of the specimen. This model utilizes white light interferometry for high-resolution 3D surface measurements. It has a vertical measurement range from 0.1nm to 1mm. The morphology of the machined surface was determined by investigating the measured data such as the surface profile, depth of machining, and the roughness pattern.

2.9 Digital Microscopy

DIGITAL MICROSCOPE VHX-5000 presented in Figure 2-10 was used for imaging micro-molds. VHX recognizes focus information automatically and creates a depth composition image rapidly. A motorized x-y stage allows the operator to quickly observe a depth composition image at the desired point. Once the sample is positioned on the stage, a depth composition image is

generated in one second at the fastest speed. Images are captured at 50 frames per second, with different focus positions, and processed at high speed by the REMAX V graphics processor. This digital microscope provides very high-quality 3D and 2D images in different angles.

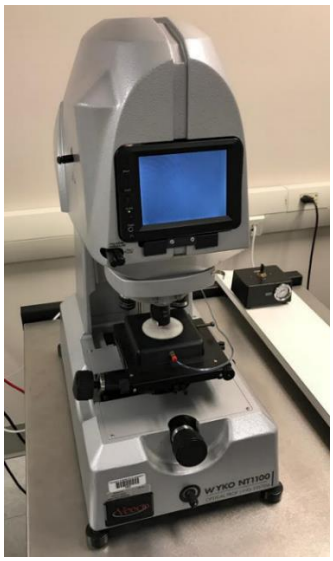

Figure 2-9. WYKO NT1100 Optical Profiling System

Figure 2-10. Digital microscope Keyence VHX-5000 [https://www.keyence.ca/].

2.10 CCD Camera

To capture the image of the micromachined samples, the light source and image recording should be placed on the same side of the sample that has been machined. For this purpose, a CCD camera (HAYEAR 12 MP USB C-mount) with a lens (HY-D100X, adjustable 8X-100X) was used for

capturing the images. LEDs were used to have sufficient and uniform light during imaging. Figure 2-11 shows the whole microscope including the camera, lens, and LEDs.

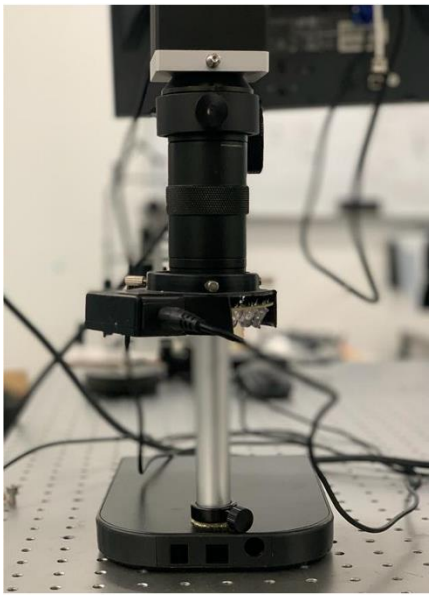

Figure 2-11. CCD camera (HAYEAR 12 MP USB C-mount)

2.11 Design of Experiments

2.11.1 Evaluation of Parameters

Various parameters such as wavelength, spot size, power, overlap, and the number of pulses can have a significant effect on the laser micromachining. Therefore, it can be concluded that by changing any of these parameters, micromachining specifications such as quality, depth, and the roughness can be varied. We keep the wavelength and beam diameter at 532 nm and 0.23 mm respectively, to study the effect of other optomechanical paramters (power, overlap, and the number of pulses) on micromachining.

The variable parameters such as power, overlap, and the number of pulses were varied to study their effect on the micromachining. An experiment was designed in which these parameters were changed successively to investigate their effects on the micromachining and ablation process by comparing them together. This experiment made it possible to examine and compare the results and effects of these parameters on the laser micromachining process.

In this experiment, some straight 1 mm horizontal lines were fabricated. In evvery condition, only one of the parameters was varied to see its effect on micromachining quality. Finally, the micromachining results were compared together based on the machining depth, machining accuracy, and surface roughness.

2.11.2 Overlap

For micromachining, three different overlaps of 0%,40%, and 80% were chosen to determine which percentage of overlap can perform the maximum quality, precision, and depth in micromachining. The produced features were examined using a microscope and an interferometer in order to select the most optimal and most appropriate overlap for the remaining investigations. The optimal decision corresponds to the highest machining accuracy, deepest cutting depth, lowest surface roughness, and resolution supplied by the required overlap. Figure 2-12 gives schematic information about the different overlap percentages. Since the increase in overlap causes more laser pulses for machining of 1 mm lines, it proportionally reduces the scanning speed as shown in Table 2-1.

Table 2-1. Pulse pitch, and scanning speed associated with three different overlap percentages

Overlap percentage	0	40	80
Laser pulse pitch (µm)	58.7	35.22	11.74
Scanning speed (µm/s)	11.7×10^5	7.04×10^5	2.35×10^5

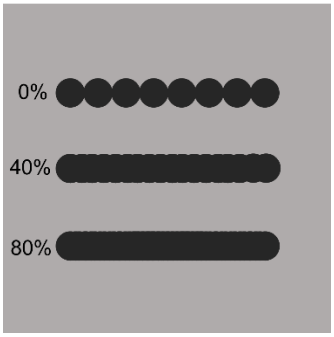

Figure 2-12. Schematic of straight-line experiments with different overlap of 0%, 40%, and 80%.

2.11.3 Number of Pulses

The number of pulses refers to how many times the laser pulses are fired at a specific location in the machining region. We could adjust the number of pulses at each spot if we could move the

laser beam in the x and y directions at the specified scanning speed, with a dwell time at each spot, as defined in table (2.5, 5, 10, 20, 200 ms/50 to 4000). By increasing the number of pulses at a certain spot, the temperature in the machining area rises, resulting in faster material removal. As a result, in laser micromachining, the number of pulses can be a critical parameter that has a direct effect on the cutting depth and micromachining accuracy.

2.11.4 Power

In the initial phase, as we do not know how much power is required for magnesium ablation, the laser power was measured after each optic to find the correct laser power that can readily ablate the sample. Therefore, a powermeter (COHERENT, LabMax-TO) was utilized to register the laser power after each optics. It is because each optical components can cause power loss due to their light absorption properties. The measured powers are mentioned in Table 2-2. In addition, Figure 2-13 depicts a schematic of laser power after each optic.

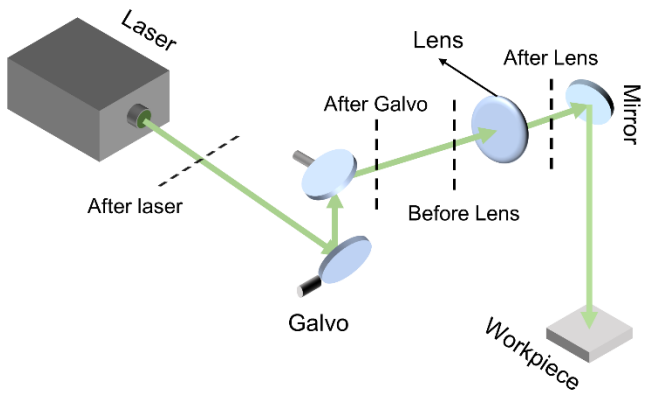

Figure 2-13. Schematic of laser power after each optic.

Table 2-2. Laser powers at different positions

After Laser	After Galvo	Before lens	After lens
370 mw	310 mw	270 mw	170 mw

Then, dividing the measured laser powers before impacting the sample (focal length) by the laser power after leaving the beam source yields a relative ratio of 0.46. Since laser power is a key parameter in laser micromachining, this ratio can assist us in selecting the appropriate power for the machining process. As a result, it was discovered that utilizing 40% laser power (1.1 W), and 45% power (2.4 W) are the optimum choices at 20 kHz repletion rate for laser micromachining

that can manufacture an acceptable depth with these optics. Therefore, these two powers were employed in all trials, and their effects on the laser micromachining were studied.

2.11.5 Spot Size Experiment

As reported in section 2.32.3, the calculated spot size in Eq. (2.1) was 58.7 μm. An experiment was conducted to ensure the accuracy of the predicted spot size in Eq. (2.1). The laser beam must move so that just one laser pulse touches the sample at each point in order to measure the spot size. The determined laser repetition rate in this work is 20 kHz. Therefore, if the mirrors move in the x and y directions so that they emit 20000 different pulses, it can be said we have 20000 machined spots apart from each other on the sample, which is called the sampling rate.

Since the exact spot size is un-known, we cannot program the galvoscanner to the right position for fabricating the perfectly tangent spots. Hence, an interval was chosen and the distances between pulses in each experiment were increased by 10 μm from 40 μm to 90 μm to estimate at what distance the fabricated dots going to be tangent to each other.

The laser power was decreased to the point where it could only form texture on the sample in order to assess the spot size. Several 1 mm horizontal lines were created on the Mg sample with different sampling rates. Based on the results, it was noticed that the spots are tangent to each other at distances of 50-60 μm. It can be concluded that the spot size measured in the experiment is approximately like the number calculated in section 2.3, which was 58.7 μm. Therefore, the spot size was 60 μm, and the remaining experiments were performed based on this spot size. Figure 2-14 illustrates a schematic of the distance between the centers of the laser spots in tangent position.

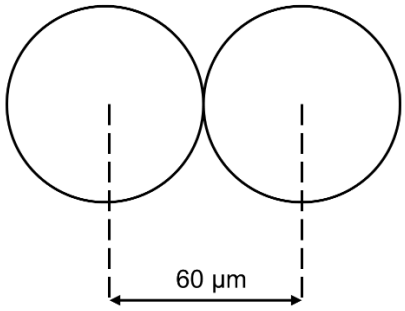

Figure 2-14 Distance between the centers of the laser spots in tangent position.

2.11.6 Opto-Mechanical Parameters Experiments

The purpose of this study is to achieve optimal parameters for 3D laser micromachining. There are two main criteria for creating 3D profiles that can be used in the industry: 1) sufficient depth 2) machining accuracy. Therefore, to demonstrate the feasibility of 3D laser micromachining, at first, it is necessary to design an experiment to evaluate the laser micromachining parameters.

In the first set of experiments, three different overlaps of 0%, 40%, and 80% were considered to investigate their effect on micromachining. In groups of three, several 1 mm horizontal lines were fabricated. The other selected parameters in this study are the power of (1.1 and 2.4 W) and the number of pulses of (400 and 4000) pulse per spot. The experiments that were carried out are listed in Table 2-3.

As 80 % overlap provided the highest micromachining accuracy and depth, the pulse overlap was kept to 80% to perform all remaining experiments in this study. In the second step, the number of pulses was varied to study its effect on the micromachining and determine the best scanning speed rate (number of pulses per spot). The number of pulses studied were (400, 200, 100 and 50) pulses per spot. All these tests were performed with the power of 1.1w and 2.4 w. Table 2-4 shows the lists of experiments that were carried out.

This experiment was carried out to determine the best number of pulses for the maximum micromachining resolution and depth. According to our research, machining with 400 pulses per spot provides the optimal micromachining performance in the manufacture of micro-profiles. Therefore, it is possible to conclude that the power of (1.1 w and 2.4 w), the overlap of 80 %, and the number of pulses of 400 pulses per spot are the most efficient parameters which are selected for performing the rest of experiments in this study.

Table 2-3. List of the first experiment and the variables

Number of Experiments	Power	Number of Pulses (pulses/spot)	Overlap
1	1.1 w	400	0 %
2	1.1 w	400	40 %
3	1.1 w	400	80 %
4	1.1 w	4000	0 %
5	1.1 w	4000	40 %
6	1.1 w	4000	80 %
7	2.4 w	400	0 %
8	2.4 w	400	40 %
9	2.4 w	400	80 %
10	2.4 w	4000	0 %
11	2.4 w	4000	40 %
12	2.4 w	4000	80 %

Table 2-4. List of the second experiment and the variables

Number of Experiments	Power	Number of Pulses (pulses/sec)	Overlap
1	1.1 w	400	80 %
2	1.1 w	200	80 %
3	1.1 w	100	80 %
4	1.1 w	50	80 %
5	2.4 w	400	80 %
6	2.4 w	200	80 %
7	2.4 w	100	80 %
8	2.4 w	50	80 %

2.11.7 2D Micromachining

Laser micromachining is a precise manufacturing technique in which accuracy is a key factor that should be considered. As mentioned earlier, the aim of this research is to achieve a high-resolution complex 3D profile. Therefore, a 2D micromachining experiment was designed to evaluate the accuracy of this optic system in fabricating complex shapes. In other words, we want to see how small dimension can be micromachined with high accuracy and resolution.

The image processing technique was used to fabricate the complex 2D geometries. The images were processed by MATLAB to guide the laser beam toward the desired coordinates. The MATLAB algorithm converts the image to a binary image. Then it determines the address of each pixel and calculates the distance between them based on the size of the image to convert them to coordinates. These coordinates are delivered to the galvanometer motors, which move the mirrors and focus the laser beam onto the sample for machining.

The mirrors move the laser beam to the desired coordinates by changing the angle. This angle change is done by galvanometer motors, which operate by changing the voltage. Therefore, Eq (2.5) was used to calculate the required voltage to move the mirrors to make the specified angle. As a result, we can move the laser beam in directions x and y to the desired coordinates on the sample. This technique allows us to create very small complex shapes with high resolution and precision through laser micromachining.

Before performing, the laser power was reduced so that the laser beam could be positioned in the right place at the corner of the sample for laser scanning. Next, the laser power was increased once again to the required power for ablation, which is 1.1 or 2.4 W. Since the laser beam starts to ablate the material at this power, an algorithm was developed in MATLAB to jump the laser beam 1mm in the x and y-axis to perform perfect micromachining. After the laser scanning has been completed, MATLAB algorithm jumps again the laser beam 1 mm in the x and y axes and stops in the opposite corner of the sample. At the end of the process, the laser power will be decreased so that the sample can be removed from the stage.

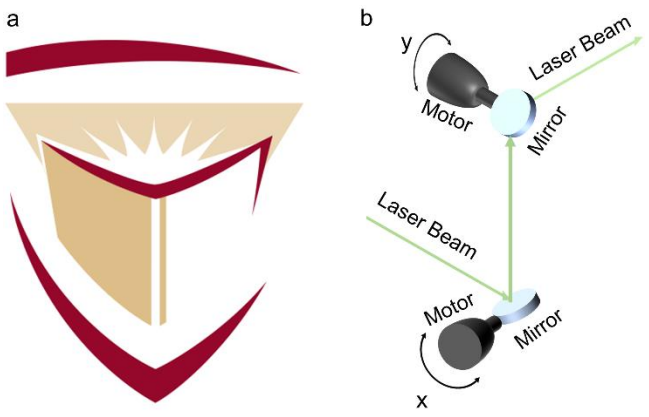

Figure 2-15. Concordia University logo. (b) Schematic of mirrors movement.

The Concordia University logo was chosen as a complex shape for this test. This geometry was micromachined in four different lengths: 1, 2, 3, and 4 mm. The purpose of micromachining in different dimensions was to evaluate the accuracy and resolution of our laser micromachining optics. Then, the samples were carefully investigated under a microscope and interferometer to assess the micromachining quality. Figure 2-15 shows a schematic of how mirrors work to fabricate the Concordia logo.

2.11.8 3D Micromachining

Fabricating the 3D micromachining profiles is the main challenge of this study. The purpose of this work is to develop a low-cost, rapid, and high-precision technique for creating 3D geometries using a laser micromachining system. Therefore, a 3D laser micromachining method was developed to fabricate complex shapes at various depths. This method was made possible by moving the laser beam in the x and y directions and moving the sample in the z direction.

According to Figure 2-3, the designed optical system consists of different optics that make 3D micromachining possible. These components include a nanosecond laser, galvanometer, converging lens, mirror, and adjustable stage in z direction. As we know from section 2.2, the galvanometer is responsible for moving the laser beam in the x and y directions. As mentioned earlier in section 2.2, the focal point forms at the distance of 20 mm after the converging lens. This means that, at this distance the laser beam has the maximum power density (as the spot reaches the minimum size at the focal plane), which makes the ablation possible. Hence, the sample should be fixed at this distance on the stage.

During each scanning step, the materials in the machining area will be ablated with a laser beam. Therefore, to achieve a deeper micromachining depth, the machined surface must be repositioned at the focal length. In each machining period, the stage was moved upwards by 20 μm in the z direction so that the sample is repositioned at the focal length to allow ablation. This technique allows micromachining in deeper layers which is called 3D laser micromachining. According to the section 2.6, a three-bar air pressure was also applied to the machining area during machining process to reduce the debris deposition inside the grooves. This allows the laser beam not to be blocked by debris and be able to reach bottom of the grooves easier.

To investigate the feasibility of 3D laser micromachining, an experiment was designed in which a pyramid was micromachined layer by layer on a magnesium sample. First, the sample was fixed on the stage at the focal length to prevent it from moving throughout the machining operation. Five layers of micromachining were performed to fabricate a pyramidal geometry. Following the machining of each layer, the stage was moved upward to reposition the sample at the focal length in order to machine the next layer. The dimension of the first layer were a square of 5mm×5mm, and in each layer of machining, the dimensions of each square were reduced by 1 mm to finally a pyramidal geometry was fabricated. During the laser micromachining, air flow was applied to the machining area. This experiment was repeated twice with two different power of 1.1 and 2.4 W. Other parameters such as the number of pulses and overlap were 400 pulses per spot and 80%, respectively.

Another experiment was designed to evaluate the accuracy of this technique for creating complex 3D geometries. Therefore, a gear shape was considered as a complex shape for the second phase of 3D laser micromachining experiment. Same as the previous test, the sample was fixed on the stage to prevent it from moving during the micromachining. Then, the sample was placed at the focal length for micromachining. Again, after scanning each layer of gear, the stage was moved upward in the z axis to reposition the sample at the focal point. During the micromachining, the air flow was applied to the machining area to reduce the debris production. This experiment was repeated twice with two different power of 1.1 w and 2.4 W too. In this experiment, similar parameters were used in the previous experiment such as number of pulses and overlap of 400 pulses per spot and 80%, respectively.

2.11.9 Micro-Molding

In the last part of this study, the samples were molded by Polydimethylsiloxane (PDMS). First, Silicone Elastomer Curing Agent and Silicon Elastomer Base presented in Figure 2-16 were combined in a weight ratio of 1 to 10 to make PDMS, respectively. To prevent the formation of bubbles inside of the final product, the mixed material was vacuumed for 15 min by the vacuum chamber to remove all bubbles. In order to facilitate the removal of PDMS from the molds after they are cured, oil was applied to the surfaces before filling them with PDMS.

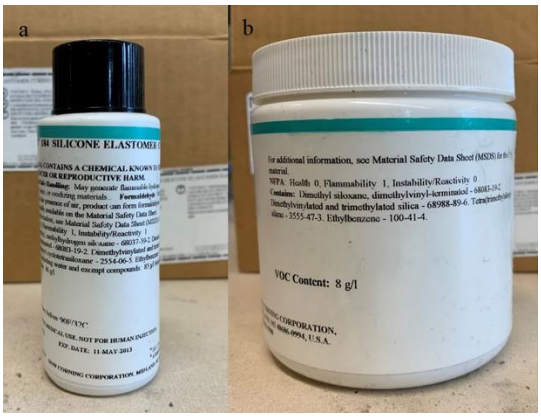

Figure 2-16. (a) Elastomer (b) Resin

After filling the samples with PDMS, the samples were vacuumed again for 15 min to remove all residual bubbles. Then, the samples were placed in the oven at 70° for 2 hours to cure the PDMS. Finally, the PDMS were removed from the mold as a final product (sample).

2.12 Summary

In this study, a laser micromachining technique was presented for fabrication of a high-resolution 3D micro profiles. This laser micromachining setup used a 532-nanosecond laser, galvanometer, converging lens, mirror, and adjustable stage as optical components. In2.3 section 2.3, the laser beam spot size was calculated by Eq. (2.1) which is 58.7 µm. Also, the Eq. (2.3) was used to find the scanning speed that can provide a certain overlap percentage. A MATLAB algorithm has been developed to control the movement of galvanometer mirrors which allows the laser beam to move in x and y axis.

Since, Magnesium (Mg) finds enormous application in construction and industry, it was selected as a sample for micromachining in this study. During the micromachining, a 3-bar air pressure was applied to the machining area to reduce debris and improve surface quality. For imaging and measuring the samples, an interferometer, confocal, bright-field imaging, and microscope were used.

To find the required power for the ablation of magnesium, laser power was measured after each optic. The optimum choices for laser micromachining at 20 kHz repetition rate were 40% laser power (1.1 W), and 45% power (2.4 W). As the repetition rate was determined 20 kHz, the mirrors were moved in the x and y directions so that they emit 20000 different tangent pulses. It was noticed that the distance between the center of two tangent spot is almost 50-60 μm that is close to the calculated spot size in Eq. (2.1).

In the first stage, some 1 mm horizontal lines (20 lines) were created consecutively. In each line the laser parameters such as overlap, power, and the number of pulses were varied to investigate their effects on micromachining. Then, the results were investigated in terms of machining depth, surface roughness, and machining accuracy. In the second stage, 2D laser micromachining was performed on four different scales in order to assess the accuracy of this optical system in fabricating complex geometries. In the third stage, the stage was moved upward towards the focal length to make possible the 3D laser micromachining. This investigation explored the feasibility and machining accuracy of this 3D micromachining technique by micromachining a pyramid and gear as a complex shape.

CHAPTER 3. 2D MICROMACHINING

In this chapter, laser parameters evaluation and 2D laser micromachining were investigated. Based on the section 2.11, numerous experiments were done on magnesium samples to study the effect of the laser parameters on the laser micromachining. Except for the wavelength and spot size, which are constant characteristics, other parameters such as power, the number of pulses, and overlap were changed in each series of experiments.

In the first part of the experiments, as shown in Figure 3-1, some straight horizontal lines with a length of 1 mm were consecutively machined with different combinations of the parameters. The selected parameters are the pulse overlap (0%, 40% and 80%), the number of pulses (50, 100, 200, 400 and 4000 pulses per spot), and the power (1.1 and 2.4 W). Finally, the results were carefully investigated based on the depth, machining accuracy, and machining speed.

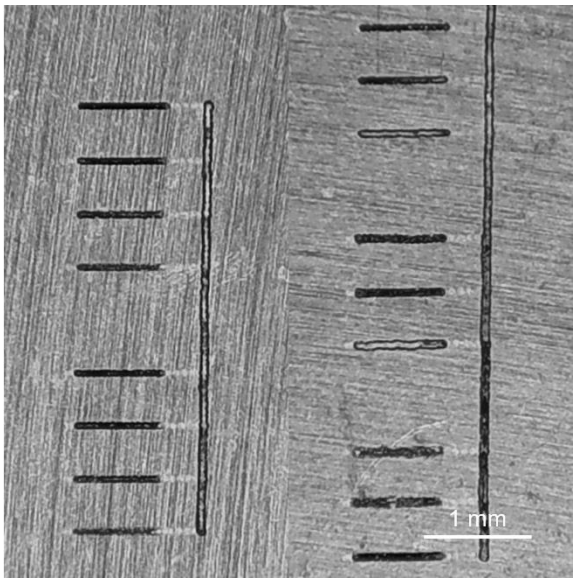

Figure 3-1. Laser micromachined lines with the various laser parameters.

In the second part, a complex geometry was chosen for performing 2D micromachining. The geometry was machined in various dimensions to get the smallest possible micromachining with this optics. Finally, the results were examined to explore the precision of micromachining in different scales.

3.1 Results and Discussion

3.1.1 Evaluation of Surface Roughness (R_a)

In this section, the surface roughness of the laser micromachining experiments is extensively investigated. Figure 3-2 depicts the average surface roughness (R_a) of the laser micromachining with the overlap of 0, 40 and 80 %, laser powers of 1.1 and 2.4 W which were performed by the number of pulses of 400 pulses per spot. Micromachining with the power of 1.1 W and the number of pulses of 400 pulses per spot showed the smoothest roughness in all overlaps. In micromachining with the power of 1.1 W, the roughness begins at 1.15 µm at the overlap of 0% and increases with a slight slope and reaches 1.33 µm and 1.89 µm at 40% and 80 % overlap, respectively.

As expected, Figure 3-2 indicates significant growth in roughness at micromachining with the laser power of 2.4 W. The roughness begins at 2.64 µm at the overlap of 0% and increases slightly and reaches 3.04 µm at 40% overlap. By increasing the overlap from 40% to 80%, the micromachining roughness increases dramatically to 5.68 µm. As laser power increases, the temperature at the micromachining area increases, causing more material melting during the ablation, which increases surface roughness. According to Figure 3-2, increasing in the laser power and overlap induces an increase in surface roughness. To investigate the effect of the number of pulses on roughness, another set of experiment was performed with a higher number of pulses.

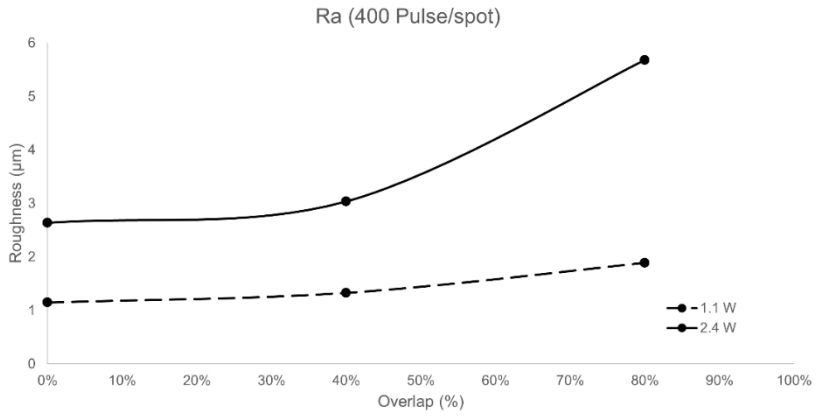

Figure 3-2. Laser micromachining roughness for the number of pulses of 400 Pulse/Spot, overlap of (0, 40 and 80) %, and the power of (1.1 and 2.4) W.

Figure 3-3 illustrates the average surface roughness (R_a) of laser micromachining with the overlaps of 0, 40 and 80 %, laser powers of 1.1 and 2.4 W which were performed by the number

of pulses of 4000 per spot. Figure 3-3 depicts a significant roughness rise in all conditions of micromachining with 4000 pulses per spot. In micromachining with the power of 1.1 W, the roughness begins at 2.50 µm at the overlap of 0% and grows with a slight slope to 2.86 µm at 40% overlap. By increasing the overlap to 80%, the roughness grows with a steep slope and reaches 5.00 µm.

Increasing the laser power to 2.4 W enhanced the surface roughness in all overlap percentages. The roughness starts at 4.28 µm at 0% overlap and grows with a uniform slope and reaches 5.16 µm and 6.39 µm at 40% and 80%, respectively. Increasing the number of pulses at a spot reduces the micromachining speed, which increases the temperature in the machining area and causes more material melting, resulting in increased the surface roughness.

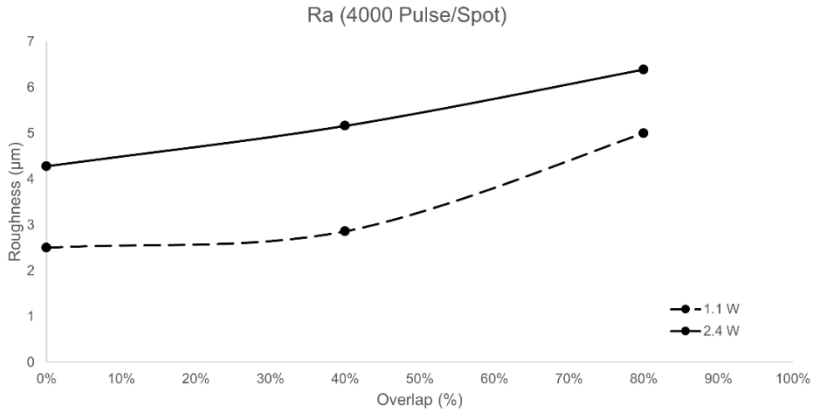

Figure 3-3. Laser micromachining roughness for the number of pulses of 4000 Pulse/Spot, overlap of (0, 40 and 80) %, and the power of (1.1 and 2.4) W.

According to Figure 3-2 and Figure 3-3, micromachining with the number of pulses of 4000 pulses/spot produces a substantially rougher surface than micromachining with the number of pulses of 400 pulses/spot. Therefore, the number of pulses of 4000 pulses per spot provides a lower micromachining quality and accuracy. Moreover, working with 400 pulses per spot causes 10 times increase in the micromachining speed compared to 4000 pulses per spot. For the line of 1 mm at 80% overlap, there needs to be 340000 pulses, which takes 17 sec to machine at repetition rates of 20 kHz. Whereas at 400 pulses per spot, it requires only 34000 pulses for the same distance of 1 mm thereby reducing the time to 1.7 sec at 20 kHz repetition rate. Moreover, the reduction of number of pulses also reduces the amount of melting and recast layer thereby increasing the machined quality. Hence, micromachining with 400 pulses per spot was selected as an optimal

condition in terms of surface roughness and speed, the rest experiments were performed with this speed.

3.1.2 Evaluation of Micromachining Depth

First, we investigated the effect of overlap on micromachining (details of the experiment are presented in section 2.11). Twelve experiments were performed with the powers of 1.1 and 2.4 W and the number of pulses of 400 and 4000 pulse/spot for the overlaps of 0%, 40%, and 80%.

Figure 3-4 provides information about the effects of the overlap on the machined depths in laser micromachining with 400 pulses per spot and the powers of 1.1 and 2.4 W. Micromachining with the 0% overlap at both powers generates the least depth against the maximum overlap of 80%. At the power of 1.1 W, micromachining depth at the overlap of 0% grows gradually from 8.58 μm to 11.18 μm at the overlap of 40%. However, the micromachining depth increases dramatically to 21.31 μm by increasing the pulse overlap to 80%.

Figure 3-4 shows a considerable growth in machining depth at 2.4 W laser power. The machining depth has sharply risen from 8.58 μm to 24.48 μm at 0% overlap. This dramatic change in depth illustrates the importance of laser power in the micromachining. Unexpectedly, a slight 3.26 μm reduction in depth is observed at 40% overlap and the machining depth was decreased to 21.22 μm. This reduction is in the range of measurement error that was observed in other experiments.

This error can be explained with the test conditions such as the sample defects or the presence of debris inside the grooves that prevent the laser beam to reach the inner layers. By increasing the overlap from 40% to 80%, the micromachining depth increases to 25.30 μm. The maximum depth can be achieved at 80% overlap regardless of laser power. At the laser power of 2.4 W with 400 pulses per pot the heat is too high that causes remelting so there is no effect of overlap on the depth.

Figure 3-5 depicts the micromachining depths for different overlaps in which the number of pulses is 4000 per spot. As expected, the depth significantly increases by increasing the number of pulses from 400 to 4000 pulse/spot. The machining depth is 20.29 μm at the 0% overlap in 1.1 W laser power. By increasing the overlap from 0% to 40 %, we observed around 3.64 μm decrease in depth (16.65 μm). Since this variation is in the range of measurement error, it can be explained by the

lack of laser pulse penetration caused by the debris. By changing the overlap to 80%, the machining depth grows gradually to 20.56 µm.

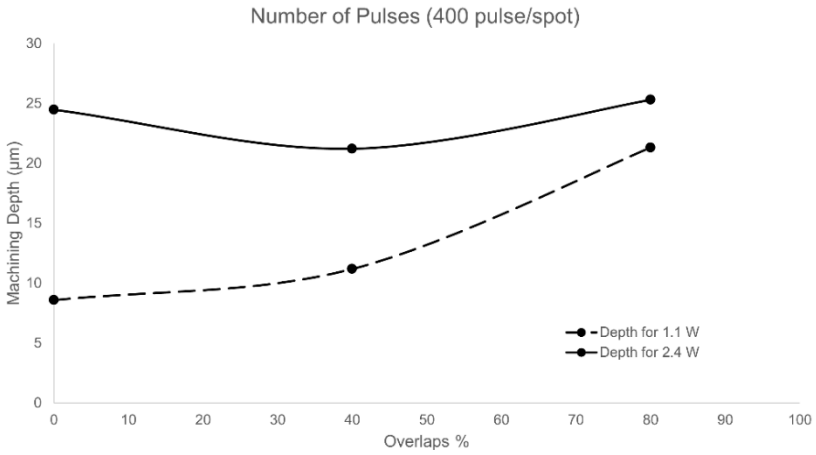

Figure 3-4. Laser micromachining depths with the variation of the overlap (0%, 40% and 80%), the NOP of 400 pulse/spot, and the power of (1.1 and 2.4) W.

Surprisingly, the depth slope is almost linear in micromachining with the laser power of 2.4 W and there is no significant change in depth at different overlaps. The depth at the 0% overlap is 22.33 µm. Moreover, machining depths for 40% and 80 % overlaps are 22.55 and 24.11 µm, respectively.

With an overview of the two Figure 3-4 and Figure 3-5, it can be concluded that by increasing the overlap the machining depth is increasing. It can be described that the number of pulses hit the specific coordinates indirectly increases by increasing the overlap. Consequently, it results in machining depth increases.

Figure 3-5 shows that in machining with the number of pulses of 4000 per spot there are no significant changes by changing the overlap regardless of laser power. Since the variation of machining depth for 1.1 W is in the range of measurement error, it can be concluded that there is negligible variation in depth regardless of pulse overlaps. Therefore, machining with 4000 pulses per spot is not applicable for 3D micromachining. To investigate the effect of the number of pulses on micromachining, we designed another set of experiment.

To study the effect of number of pulses, the overlap was kept at 80% and the numbers of pulses varied to 50, 100, 200, 400 and 4000 pulses per spot. Totally eight experiments were conducted with two laser powers of 1.1 W and 2.4 W. (details can be found in

Table 2-4)

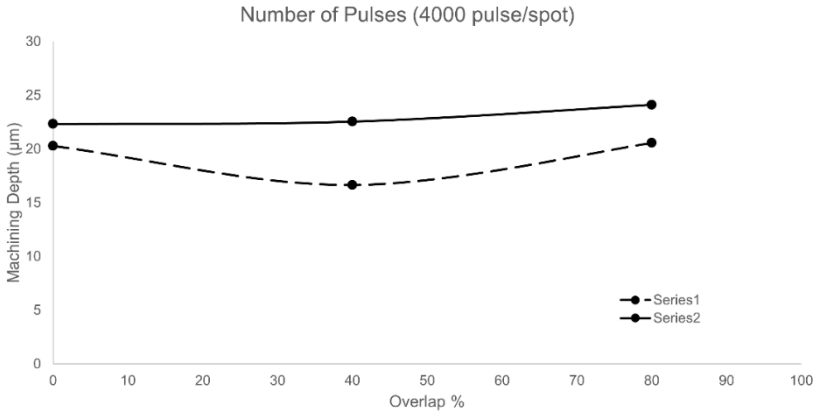

Figure 3-5. Laser micromachining depths with the variation of the overlap (0%, 40% and 80%), the NOP of 4000 pulse/spot, and the power of (1.1 and 2.4) W.

Figure 3-6 shows the machining depth for different number of pulses (from 50 to 4000 pulses per spot) and 1.1 and 2.4 W laser powers. Changing the number of pulses from 50 to 400 increases the machining depth. However, there is no significant change in machining depths between 400 and 4000 pulses per spot. Thus, machining with 4000 pulse/spot is not beneficial since it slows down the machining speed by 10 times (compared to 400 pulses per spot) without adding significant changes in machining depth.

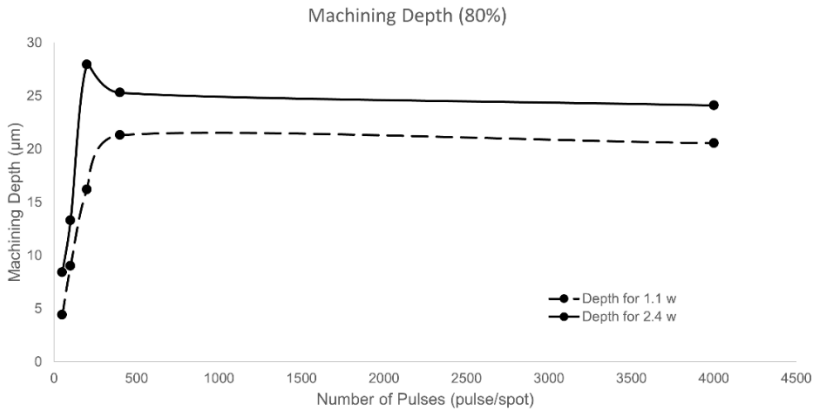

Figure 3-6. Laser micromachining depths with the different NOP of (50, 100, 200, 400 and 4000) pulse/spot, 80% overlap, and the power of (1.1 and 2.4) W.

Figure 3-7 indicates the machining depth versus the number of pulses from 50 to 400 pulses per spot. Looking at the machining depth with 1.1 W laser power, it can be concluded the greater number of pulses, the deeper the machining depth. The machining depth for 50 pulse/spot is 4.42 µm and it is the least depth that was achieved. 9.01 µm and 16.21 µm depths were achieved for

100 and 200 pulse/spot, respectively. Besides, the machining depth slightly increases to 21.31 µm at 400 pulse/spot.

The minimum achievable machining depth for 2.4 W laser power is around 8.41 µm for 50 pulse/spot which is almost equal to the depth obtained in 100 pulse/spot and 1.1 W laser power. This equality in the machining depth indicates significant effect of laser power on the machining depth and speed. The depth rises to 13.29 µm at 100 pulses/spot and it reaches the maximum achievable depth of 27.94 µm at 200 pulse/spot. By changing the number of pulses to 400 pulse/spot, the trend slightly drops to 24.30 µm depth. Since the variation in machining depth between 200 and 400 pulses is in the range of measurement error, it can be said that there is no significant change in the machining depth between these two machining conditions at 2.4 W laser power. Overall, it can be concluded that the growth in the number of pulses causes more material ablation. In turn, it increases the machining depth.

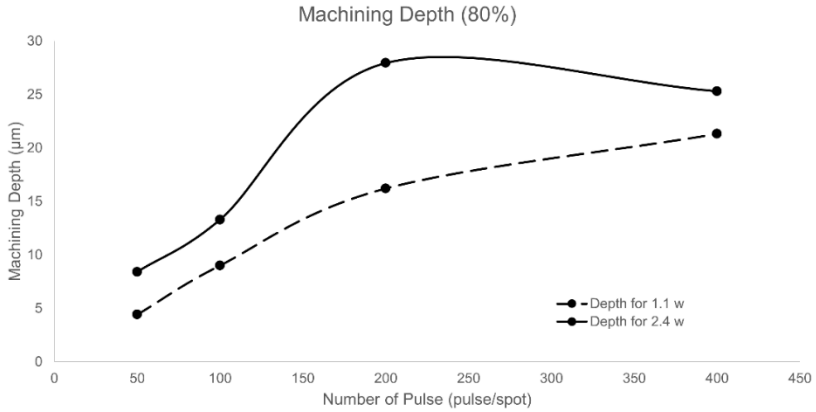

Figure 3-7. Laser micromachining depths with the different number of pulses (50, 100, 200 and 400 pulse/spot), 80% overlap, and the power of (1.1 and 2.4) W.

Our investigation shows that the laser power plays a major role on the micromachining depth. By changing the power from 1.1 to 2.4 W in all experimental conditions, a significant growth in machining depth was observed which can confirm the effect of laser power in the micromachining. Here, we seek to investigate how laser power affects the machining depth.

To ablate the material using laser, the irradiance must exceed the ablation threshold. The irradiance profile of the laser used in this study is Gaussian. Increasing the laser power broaden the part that the irradiance is higher than the ablation threshold in laser spatial profile (presented in Figure 3-8). By increasing the laser power, the radiation intensity at the center of the beam increases, which

results in greater machining depth. Figure 3-8 explains the reason for the considerable changes in machining depth changing the laser power in the experiments.

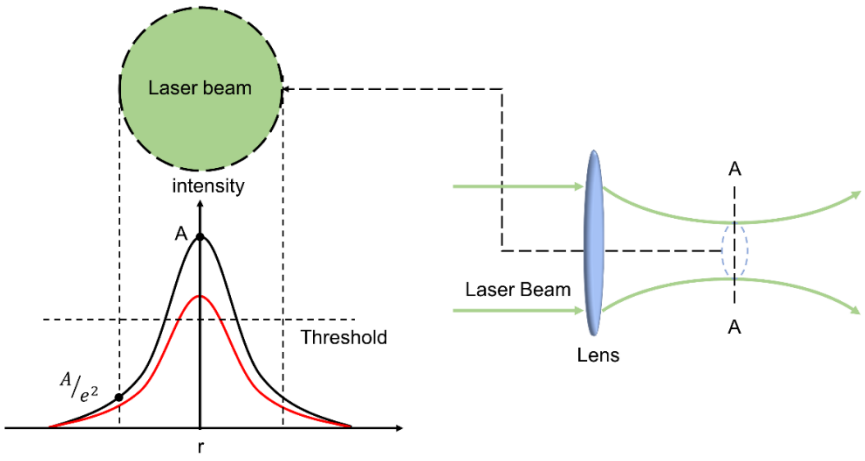

Figure 3-8. Gaussian beam behavior

Figure 3-9 provides an overview of the micromachining depths to compare the effect of laser parameters on micromachining depths. Machining with 1.1 W laser power and 400 pulses per spot creates wider machining depth range compared to other experimental conditions. Machining with 80 % overlap offers around 21 µm depth, which is roughly equal to the maximum achievable depth with the higher laser power (2.4 W). It indicates that the maximum depth can be achieved by a less powerful laser which decreases the production costs.

The effect of laser power on machining depth with 2.4 W is obvious in both numbers of pulses. The machined depths in all overlaps are much deeper than the power of 1.1 W which proves the significant effect of power parameter on the machining process. The deepest micromachining obtained with the power of 2.4 W, the overlap of 80%, and the number of pulses of 400 pulse/spot which is 25.5 µm.

Looking at machining with the number of pulses of 4000 pulse/spot, it is obvious that there are no noticeable changes in results compare to the machining with the number of pulses of 400 pulse/spot. Figure 3-9 depicts that the number of pulses more than 400 results in a linear behavior regardless of laser power. Therefore, machining with the number of pulses above the 400 pulse/spot is not beneficial.

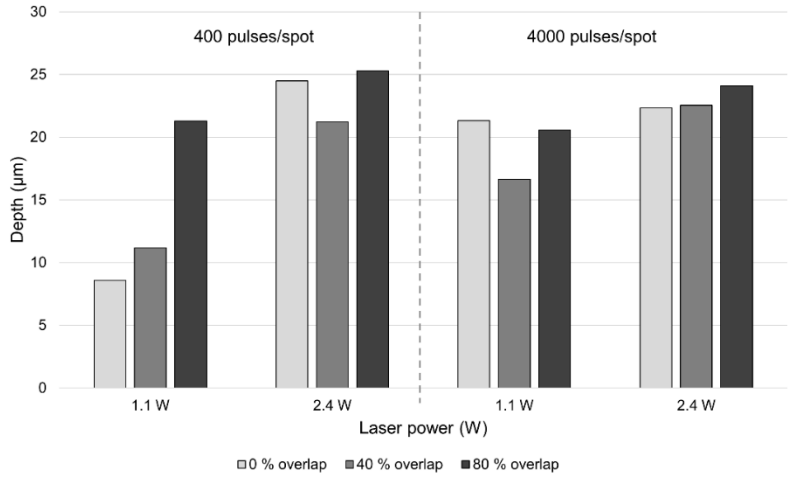

Figure 3-9. All obtained depths with the power of (1.1, 2.4) W, overlaps of (0%, 40% and 80%), and the number of pulses of (400 and 4000) pulse/spot

3.1.3 Evaluation of Micromachining Accuracy

Machining precision is another key factor in laser micromachining. In this part, we investigate the micromachining accuracy and edge quality on the above-mentioned tests. Figure 3-10 depicts the generated micro profiles under different laser micromachining conditions, which performed with 400 pulses per spot. Figure 3-10 (a) and (b) shows the micromachining with 1.1 W and 2.4 W laser power, respectively, for 0%, 40% and 80% overlaps.

Micromachining with 0% overlap in both laser powers is incapable of producing a uniform profile. This is because the laser pulses have no overlap and create separate spots on the sample. Moreover, Since, increasing the laser power improves the ablation, the machining spot size gets larger in micromachining with 2.4 W laser power, resulting in more uniform micromachining than the lower power. As the percentage of overlap increases to 40% and 80%, the micromachining accuracy and uniformity improve in both laser powers. As previously illustrated in Figure 2-4, increasing the overlap creates more laser spot interferences, resulting in greater micromachining uniformity and accuracy. Hence, increasing the overlap improve the edge quality of micro profiles.

Figure 3-11 illustrates the generated micro profiles were performed with 4000 pulses per spot, 0%, 40% and 80% overlaps, and laser powers of 1.1 W and 2.4 W. Increasing the number of pulses increases the cumulative laser irradiation at the machining area which causes more material ablation and larger spot size. Therefore, by comparing Figure 3-10 and Figure 3-11, micromachining with 0% overlap and 4000 pulses per spot has more uniform profile than the 400

pulses per spot in both powers. As expected, same as Figure 3-10, by increasing the overlap percentage to 40% and 80% the micromachining accuracy and edge quality improves significantly. Micromachining with the overlap of 80% produces the most accurate micro profiles and the best edge quality in both number of pulses.

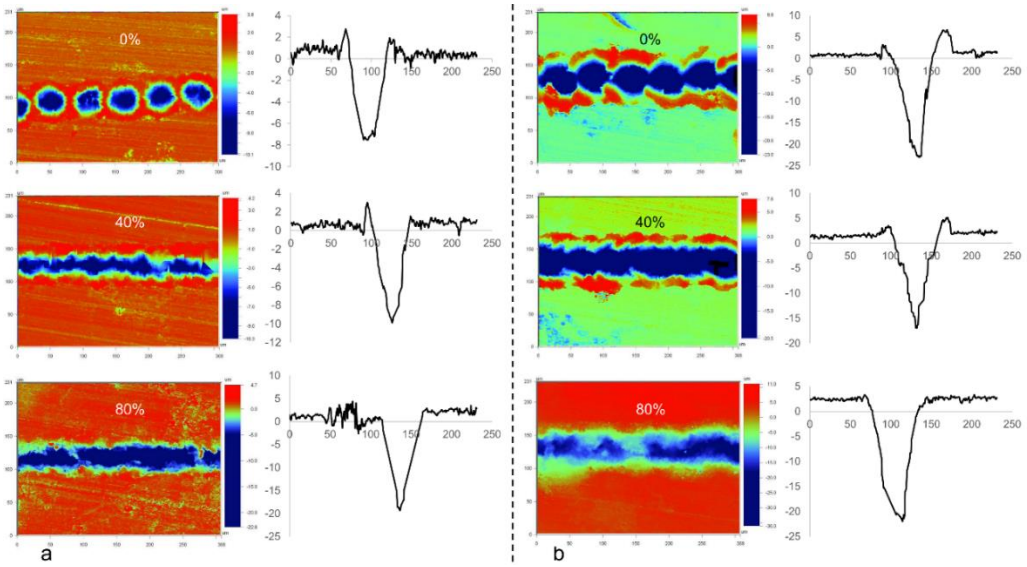

Figure 3-10. Laser micromachined profiles with the number of pulses of 400 Pulse/Spot in different overlaps of (0%, 40% and 80%): (a) laser power of 1.1 W, (b) laser power of 2.4 W.

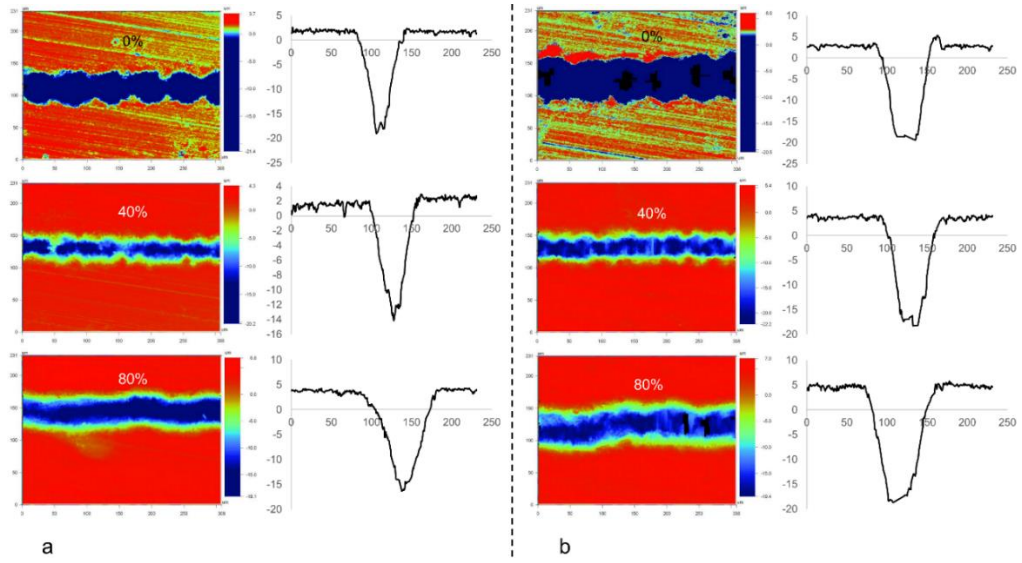

Figure 3-11. Laser micromachined profiles with the number of pulses of 4000 Pulse/Spot in different overlaps of (0%, 40% and 80%): (a) laser power of 1.1 W, (b) laser power of 2.4 W.

Evaluation of the laser parameters experiments indicates that, micromachining with 400 pulses per spot, overlap of 80% provides the most efficient laser micromachining in both powers (1.1 and 2.4

W). The micromachined profiles made with these conditions have the deepest and the most accurate with the least surface roughness. Hence, these parameters have been chosen to perform all remaining experiments such as 2D and 3D laser micromachining in this study.

3.2 2D Micromachining of Complex Shapes

A 2D laser micromachining was designed to evaluate the precision of our optical setup for fabrication of micro-structures. For this purpose, the Concordia University logo was selected as a complex shape for this experiment. Since the aim of this experiment is to investigate 2D laser micromachining, only 1.1 W laser power was used to perform this test. As described in section 2.4, MATLAB algorithm receives the image to process before guiding the laser beam to the desire micromachining coordinates.

In the first experiment, a sample with a dimension of 4×4 mm was selected to be machined with the laser power of 1.1 W, the overlap of 80%, and 400 pulses per spot. Figure 3.11 provides information about the 2D micromachined profile along with the logo. The results indicate that the laser micromachining system showed a convincing performance to fabricate the details in 2D micromachining. Comparison between Figure 3-12 (a) and (b) indicate that the features in logo such as corners and inner and outer curves were machined with micrometric precision.

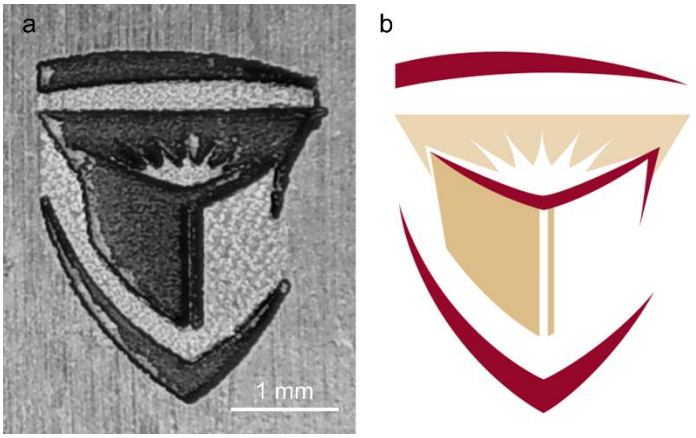

Figure 3-12. 2D laser micromachining: (a) micromachining result (b) Concordia University logo

Another experiment was designed for further investigation on the quality and precision of laser micromachining, in which the Concordia University logo was micromachined in various dimensions to find the smallest dimension that could be generated with the optical setup. Figure

3-13 illustrates the micromachined samples in four different dimensions as 4×4 mm, 3×3 mm, 2×2 mm, 1×1 mm, and their confocal images. An overview of Figure 3-13 indicates that our laser micromachining system performed a high resolution of micromachining in all scales.

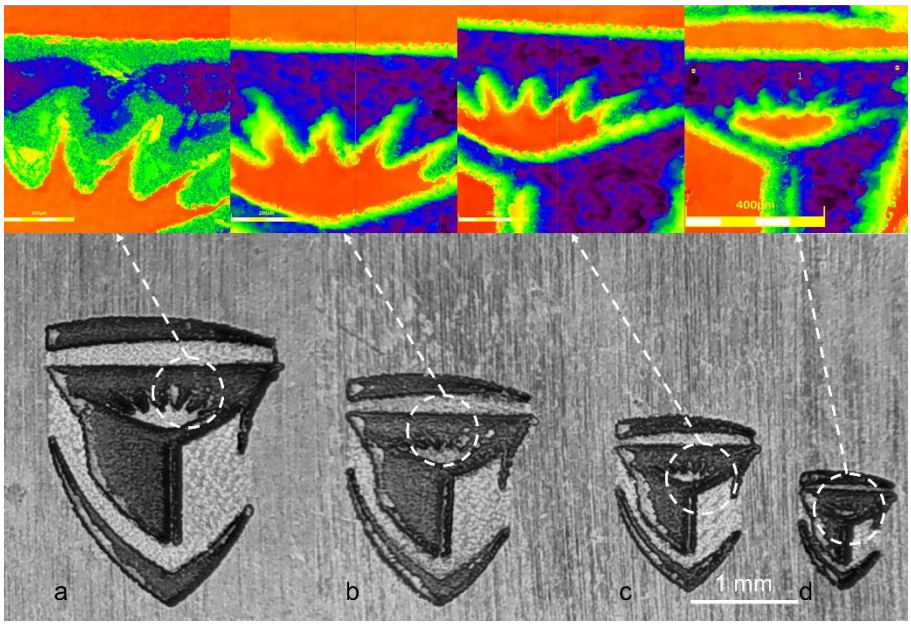

Figure 3-13. 2D micromachining and confocal images: (a) 4×4 mm (b) 3×3 mm (c) 2×2 mm (d) 1×1 mm.

According to Figure 3-13, image (a) is the largest sample that we micromachined with this setup. The laser micromachining system shows a high precision when it comes to creating features such as corners and curves. Micromachining of 3×3 mm illustrated identical micromachining resolution and accuracy to 4×4 mm logo.

As predicted, the resolution and accuracy of micromachining decreases as dimensions reduce. Figure 3-13 (d) depicts the smallest possible micromachining size that we fabricated with this optical setup which is 1×1 mm. By comparing the images (d) and (a), as the dimensions of profiles become smaller, the precision and resolution of micromachining decreasing considerably.

The reduction in micromachining resolution in small dimensions is due to the features that are smaller than the laser spot size. Therefore, the laser beam is unable to precisely machine all micrometric features such as corners. As mentioned in section 2.3, the calculated spot size by Eq. (2.1) was 58.7 µm. This is the main reason for the reduction in micromachining resolution in smaller scales. The reason for the 1mm×1mm being the smallest size is due to the fact that at this

scale the finest details in the logo reach the spot size of the laser. So, anything smaller than this would not be possible with our current setup. This problem can be solved by replacing lasers that produce smaller spot sizes or using lens with higher numerical aperture (NA). When lenses with smaller spot size are used the focal length is going to be reduced and this reduces the scan area. With 200 mm focal length lens we could get the scan area of 10 mm×10 mm.

In the next step, all 2D micromachined samples were carefully scanned and examined under the confocal microscope. Figure 3-14 illustrates average surface roughness (R_a) in all above-mentioned 2D constructs with different scales. Since all samples were micromachined under the same optomechanical parameters, their surface roughness is approximately in the same range, with a maximum variance of 0.8 µm.

For 4×4 mm construct, the average surface roughness of micromachining is 3.64 µm. Despite the micromachining of larger scales should have a smoother surface compared to the smaller scales, the roughness of the 4×4 mm sample is 0.59 µm higher than the 3×3 mm sample, which is 3.05 µm. This disagreement in the result is within the measurement error range, which can be explained by sample defects and the lack of laser pulse penetration induced by debris.

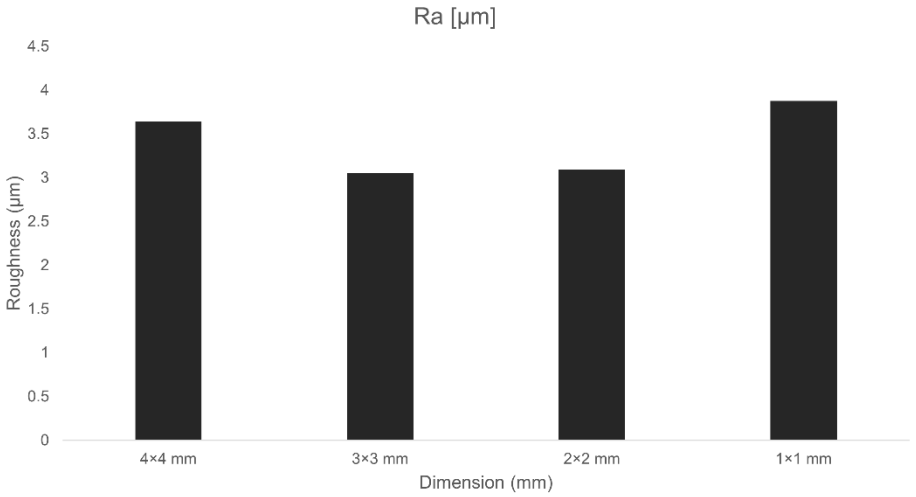

Figure 3-14. The roughness of Concordia University logo in various scales

By decreasing the micromachining size from 3 mm to 2 mm, the roughness increases slightly to 3.09 µm. As expected, the roughness of the 1 mm sample rises dramatically from 3.09 µm to 3.88 µm (highest surface roughness among all 2D micromachining). As discussed earlier, as the micromachining scale is reduced, the geometry's details become smaller than the spot size.

Therefore, we were not able to precisely machine the smallest construct with high precision which results in the surface roughness increase.

Looking at Figure 3-15, the depth variation follows approximately the same trend as the roughness graph. As discussed in sections 3.1.2, there is a direct relation between surface roughness and micromachining depth. The depth begins from 23.39 µm at the 4 mm scale and decreases significantly to 15.98 µm and 15.06 µm at 3 mm and 2 mm scales, respectively. As predicted, by increasing the roughness at 1 mm scale, the micromachining depth was increased and reached 22.87 µm.

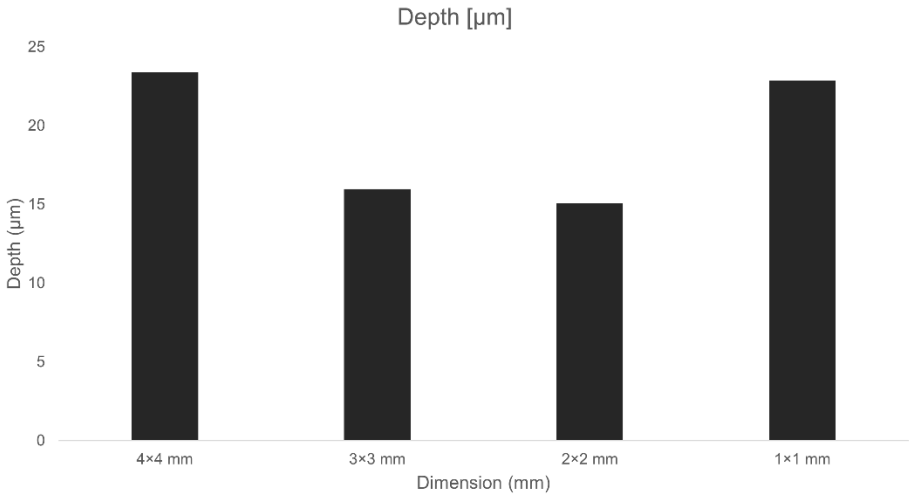

Figure 3-15. The depths of Concordia University logo in various scales

3.3 Summary

In this chapter, an experiment was designed to evaluate the effect of the laser parameters such as power, overlap, and the number of pulses on micromachining. A series of 1 mm lines were successively machined with varying parameters. All experiments were conducted with two laser powers of 1.1 and 2.4 W. To observe the effect of overlap, in the first experiment, the overlap was changed from 0, 40, and 80% with the number of pulses as 400 and 4000 pulses/spot. Micromachining with 80% overlap and 400 Pulses/Spot was found to be the most efficient parameter combination for both laser powers in terms of machining depth, surface roughness, and machining accuracy. In both laser powers of 1.1 and 2.4 W, the surface roughness at 80% overlap are 1.89 m and 5.68 m, and machining depths are 21.31 m and 25.30 m, respectively. In

micromachining with 80% overlap, the laser beam has a greater overlap than 0 and 40% and performs a more uniform machining process.

In the second experiment, to investigate the effect of the number of pulses on micromachining, the overlap was kept at 80%, and the number of pulses varied between 50, 100, 200, 400 and 4000 Pulses/Spot. The machining depth increased by increasing the number of pulses up to 400 Pulses/spot. But the machining depth did not have a sensible change by increasing the number of pulses from 400 to 4000 Pulses/spot and it was 20.56 µm and 24.11 µm at two powers of 1.1 and 2.4 W, respectively. This means that micromachining with 4000 Pulses/spot is not beneficial. Also, micromachining with 4000 Pulses/spot created a much rougher surface compared to micromachining with the number of pulses of 400 Pulses/Spot and it was 5.00 µm and 6.39 µm at two powers of 1.1 and 2.4 W, respectively.

Next step, a 2D laser micromachining experiment was designed to evaluate our optical system in creating 2D complex shapes. Concordia University logo was selected as a complex shape for this experiment. This shape was machined in four different scales of 4, 3, 2, and 1 mm to investigate the machining accuracy in different dimensions. The 1mm sample is the smallest scale that we tried to micromachine in this experiment. This laser micromachining system showed a good performance in all dimensions. Then, all four samples were investigated in terms of machining accuracy and surface roughness with confocal carefully.

As mentioned before, the ultimate goal of this study is to present a 3D laser micromachining system. All performed experiments in this chapter were required to be investigated before starting 3D micromachining. In the next chapter, we are going to present a 3D laser micromachining method and discuss the results.

CHAPTER 4. 3D MICROMACHINING AND MICRO-MOLDING

3D laser micromachining is a nonconventional subtractive micromachining method that fabricates 3D microstructures by ablating materials with laser beams. 3D laser micromachining provides great flexibility for creating complex microstructures at high speed, high precision, and low cost. Furthermore, no tools are needed in this method as in conventional micromachining methods, hence, there is no contact between sample and machining device, and no additional tooling expenditures. All these advantages motivated us to study and adapt a new optical setup for 3D laser micromachining.

Since the maximum laser power is generated at the focal length, the machining area should always be placed at the focal plane to let the laser machine the surface. Therefore, ablation of materials after each set of micromachinings generates a gap between the micromachining area and focal plane that makes it impossible to micromachining at greater depths. This is a major challenge in the fabrication of 3D microstructures.

To overcome the above-mentioned challenge in 3D micromachining, an adjustable stage in z-direction was used to precisely move the sample towards the focal plane. Moreover, to improve the surface quality and 3D micromachining accuracy, it was decided to apply air jet to the micromachining area to push the debris away from the machining area. First, a 5-layer pyramid was machined to investigate the feasibility of the presented approach for 3D micromachining. Then, a gear was selected as a complex shape for 3D laser micromachining to study the precision and quality of the method in fabrication of fine details. Finally, for proof-of-concept, all these fabricated samples were molded by PDMS.

4.1 Results and Discussion

4.1.1 3D Laser Micromachining Feasibility

In the first step, a 5-layer pyramid was micromachined in a layered manner with 5 different scales using 1.1 W laser beam, 80 % overlap and 400 pulse per spot. The air jet was applied to the micromachining area to enhance the micromachining quality. The first micromachined layer was a 5×5 mm square. Then, the stage was moved 20 μm towards the laser focal plane in the z-direction for performing the next micromachining layer, which is a 4×4 mm square. This process was repeated five times, with 1mm size decrease in x and y directions. The last layer was a 1×1 mm square, which is the deepest layer of micromachining in this experiment. Figure 4-1 shows the

micromachined pyramid. As can be seen, the presented technique in this study made the 3D laser micromachining feasible. A closer look at Figure 4-1 reveals that the quality of the edges and corners reflects a high precision of 3D micromachining performance in each layer.

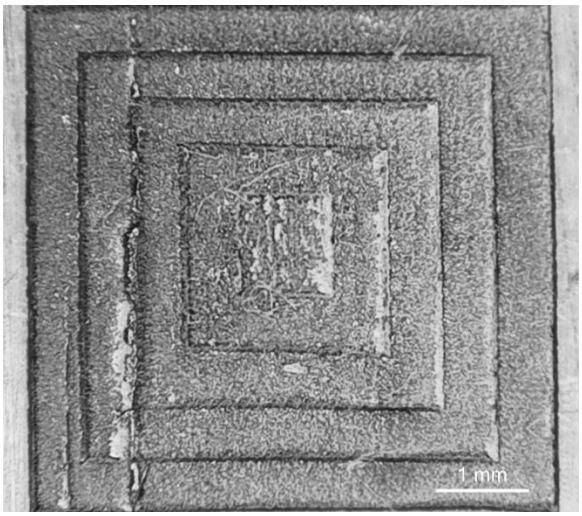

Figure 4-1. Pyramid 3D laser micromachining (Power: 1.1 W, Overlap: 80%, Number of Pulses 400 Pulse/spot)

A similar experiment was carried out with 2.4 W laser power to go deeper into 3D micromachining. Figure 4-2 (b) indicates the 3D micromachining of pyramids with 400 pulses per spot, 80% overlaps, and 2.4 W laser power. The first micromachining layer was a 6×6 mm square, and its dimensions were reduced by 1 mm per layer in each step as the stage was moved towards the focal point in the z-direction to reach a 1×1 mm square in the last layer. Similarly, the air flow was applied to the machining area for improving the micromachining efficiency.

Figure 4-2 illustrates a comparison of 3D micromachining of pyramids with 1.1 and 2.4 W laser powers. A closer look at Figure 4-2 reveals that micromachining in both conditions can fabricate a high-quality 3D microstructure. Comparison between Figure 4-2 (a) and (b) presents that micromachining with a higher laser power generates deeper microstructures. In both powers, the 3D laser micromachining system shows a high capability of creating microstructure features including edges and corners in various layers with high precision and quality.

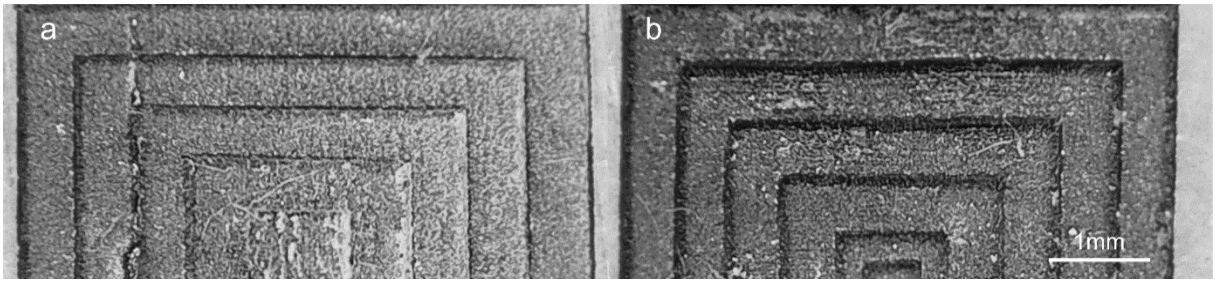

Figure 4-2. 3D micromachining of pyramids with two different laser power of: (a) 1.1 W, (b) 2.4 W.

To investigate the effect of airflow on micromachining, the airflow was adjusted to cover half of the micromachining area. Figure 4-3 depicts the result of applying airflow into the micromachining area. Figure 4-3 (a) and (b) indicate that airflow has a considerable influence on increasing micromachining quality by pushing the debris away from the machining area.

When the laser ablates the materials, the ablated materials cannot be readily removed from the fabricated grooves. Therefore, these materials stayed and exposed to the laser beam and prevented the laser beam from the machining area, as seen in Figure 4-3 (b). Also, they prevent the laser beam from reaching the deeper layers required for 3D micromachining. On the other hand, as shown in Figure 4-3 (a), air jet can reduce HAZ which prevents the materials from melting, resulting in micromachining with high accuracy and quality.

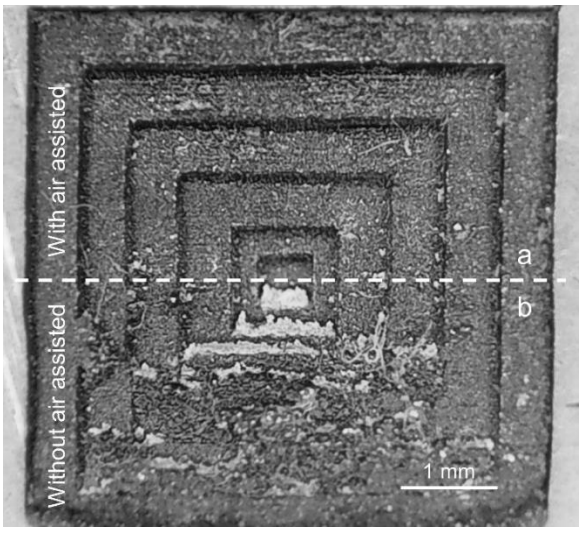

Figure 4-3. 3D laser micromachining: (a) with air assisted (b) without air assisted.

The pyramid sample performed with the higher laser power was measured carefully under the interferometer for a thorough investigation. To study the micromachining quality for

manufacturing of 3D microstructures, different portions of the pyramid in different layers, such as edges and corners, were scanned. Figure 4-4 indicates the details of the pyramid scanning in various regions. As can be seen, our modified 3D laser micromachining system can produce a high-accuracy microstructure at various depths.

As shown in Figure 4-4, micromachining of the 1st and 2nd steps provides the best micromachining accuracy in the fabrication of features such as corners and edges. The micromachining quality decreases significantly at greater depths since part of the laser beam can be blocked by the edges. Micromachining in deeper layers increases surface roughness and decreases laser penetration, which makes fabricating features more difficult than in primary layers. Our optical system provided acceptable micromachining precision at the deepest layer, which is the 5th step. Since the 6th layer of the pyramid was too deep, the interferometer was unable to scan it.

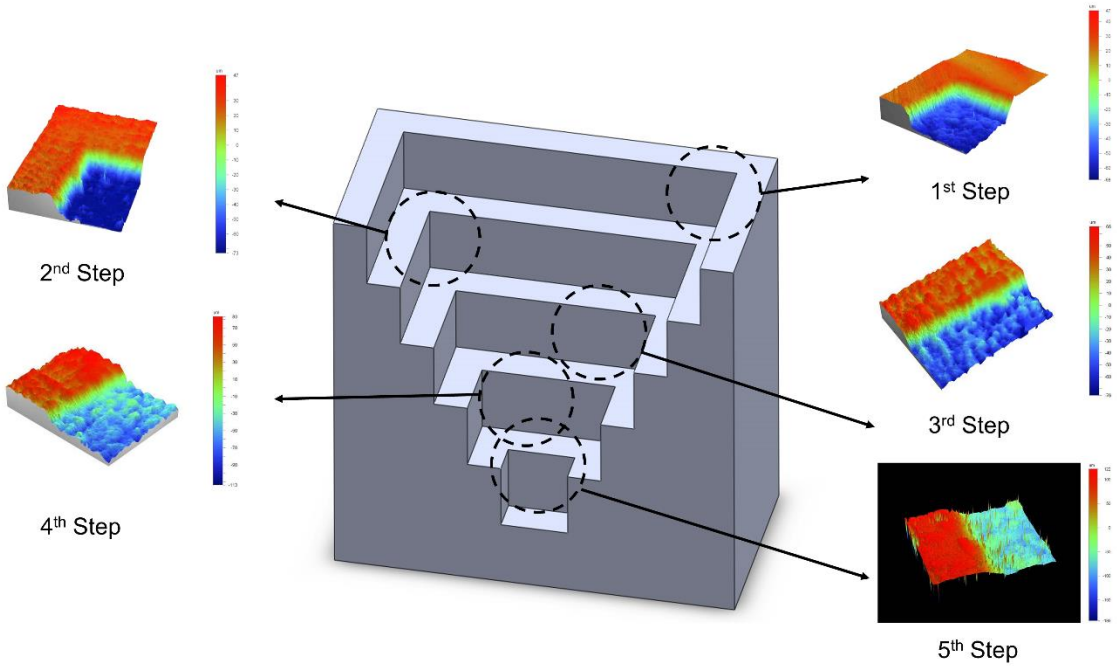

Figure 4-4. Different scanned parts in various layers of the pyramid.

Different layers of the pyramid were measured and investigated in terms of their surface roughness. Figure 4-5 illustrates the roughness measurements using the interferometer for all five layers of the pyramid which is machined by 2.4 W laser power. As predicted, the first layer has the lowest roughness among all layers (28.62 µm). the roughness of 2nd and 3rd steps slightly increases to 37.12 µm and 39.99 µm, respectively. Surface roughness at the 4th step sharply increased and

reached 51.08 µm. At the 5th step of micromachining, we see a significant increase of 21.65 µm in roughness again which ended up to 72.73 µm roughness.

By micromachining deeper layers, the surface roughness increases due to the roughness of previous layers (i.e., machining on the rough surface) and the laser beam blocking by the edges. Moreover, the laser beam exposed the ablated materials resulting in more debris production and an increase of surface roughness. As mentioned before, we could decrease (but not eliminate) the impact of this phenomenon on micromachining quality by applying the air jet into the machining area. According to the results, adding the airflow into the machining area improved the surface and micromachining quality.

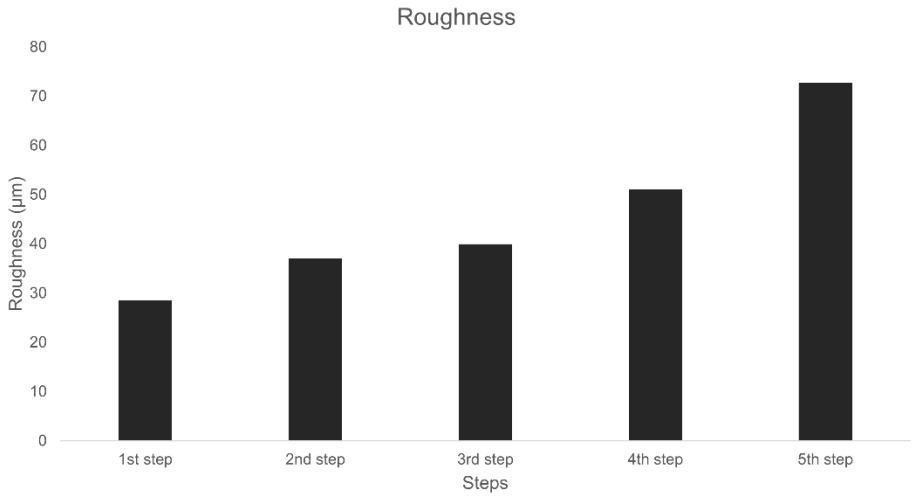

Figure 4-5. Surface roughness of the pyramid in five different layers.

Furthermore, the depth of the pyramid was measured by using the confocal microscope. Figure 4-6 gives information about the pyramid 3D profile and the micromachining depth variation. As can be seen in Figure 4-6 (a), the whole profile was scanned, and the depth of each step was measured. According to Figure 4-6 (b), as the laser parameters were constant for each set of micromachinings, the micromachining depth for each layer was 195. 03 µm ± 29.32 µm. In addition, the total depth of the pyramid from the 1st step to the 4th step was measured 778.79 µm.

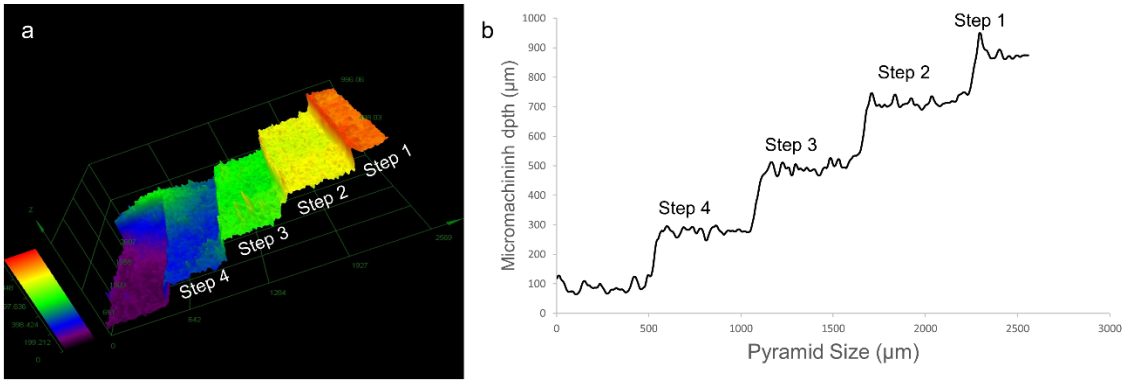

Figure 4-6. (a) Confocal image of the pyramid's 3D profile. (b) The depth variation in each step.

4.1.2 3D Laser Micromachining Accuracy

Another major challenge was whether the method can accurately micromachine the complex shapes in 3D. An experiment was designed to evaluate the ability of our approach to create complex shapes and investigate the effect of 3D laser micromachining on creation of small features. A gear was selected as a complex shape for testing the fabrication of micromachining features including corners, internal and external curves, and edges. The experiment was performed twice at two different laser powers (1.1 W and 2.4 W) with 400 pulses per spot and 80% overlap. Gears were machined in a square of 4×4 mm.

Like the previous experiment, the sample was fixed to the stage to prevent it from moving during micromachining. For each set of micromachinings, the stage was moved in the z-axis towards the focal plane to place the sample at focal length to make 3D micromachining possible. A 3-bar air jet was also used to improve the micromachining quality and push the debris away from the machining zone. Figure 4-7 illustrates the results of the micromachined samples in two different laser powers.

Figure 4-7 indicates a highly accurate 3D laser micromachining in both laser powers. All the details, such as corners, edges, and curves, were well micromachined with micrometric precision. This shows that, this optical system is accurate enough to produce the image features in a precise manner. In order to analyze micromachining details in detail, samples were scanned with the interferometer to record their surface roughness, depth, and quality. Both micromachined gears with the powers of 1.1 W and 2.4 W were scanned by the interferometer. Figure 4-8 provides information about the fabricating of small features with 3D laser micromachining. The laser was able to micromachine the gears feature such as teeth and their curvatures with micrometric

precision in both laser powers. This level of precision in laser micromachining confirms that this method is a promising alternative for other micromachining methods.

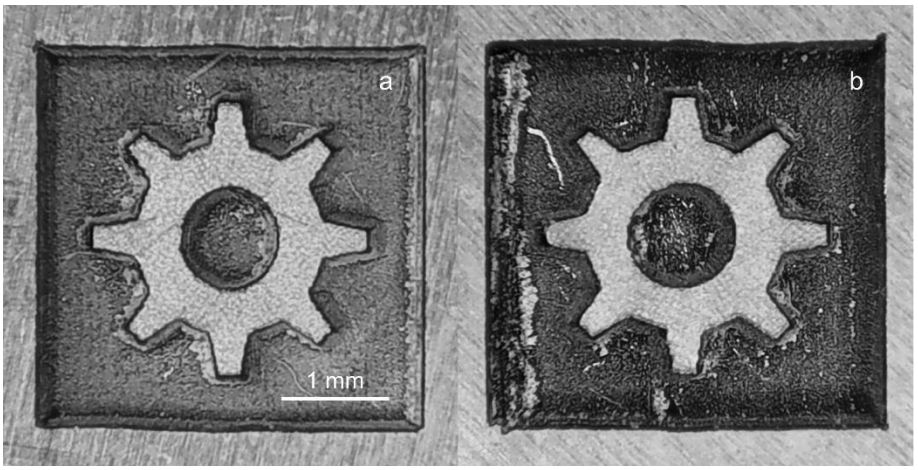

Figure 4-7. 3D laser micromachined gears with two different laser power of (a) 1.1 W (b) 2.4 W.

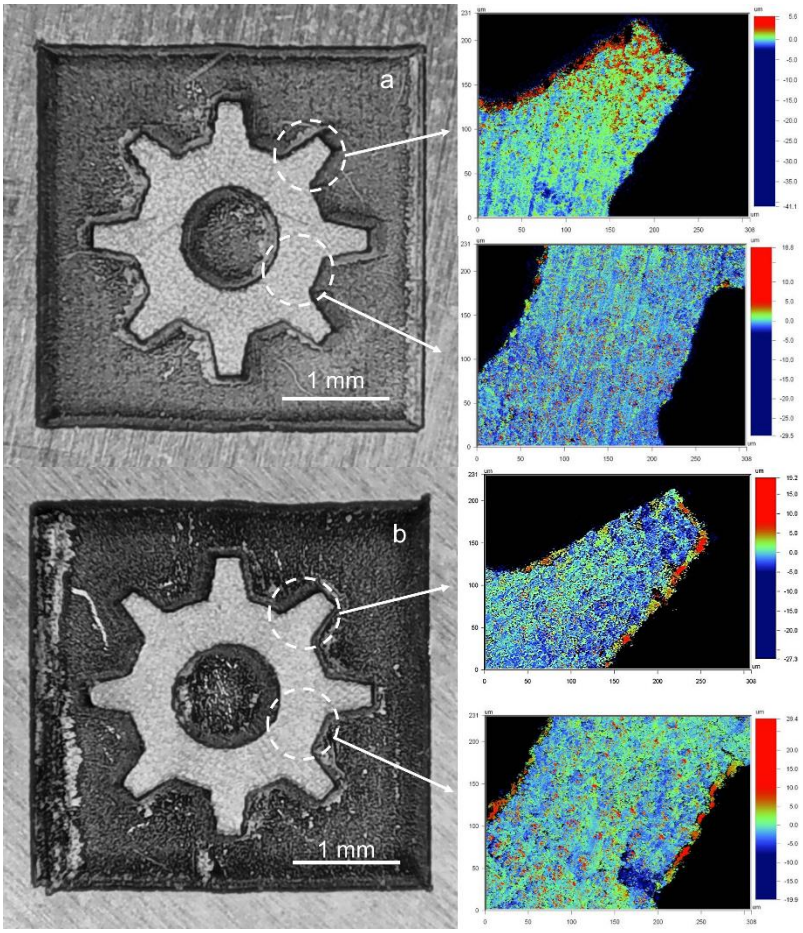

Figure 4-8. Scanning the 3D laser micromachined gear by interferometer: (a) 1.1 W (b) 2.4 W.

4.1.3 Micro-molding

Since the main focus of this study is to fabricate the 3D micro-mold, we sought to validate whether the sample mold can be used for fabrication of PDMS structure. For this purpose, PDMS have been poured to the mold cavity. After the solidification, structures were taken off the molds for imaging purposes. Figure 4-9 show the gear and pyramid molds along with the PDMS parts taken from the molds, respectively. As can be seen, the micrometric features such as corners and edges were accurately fabricated. As expected, the roughness of the machining zone affects the roughness of the PDMS structures. Moreover, the recast layer around the edges affected the roughness of the mold can impact the straightness of the edges.

This observation proves that the approach presented in this study can be an affordable and less laborious alternative for fabrication of micro-structure like hand watch parts and mold for microfluidic purposes.

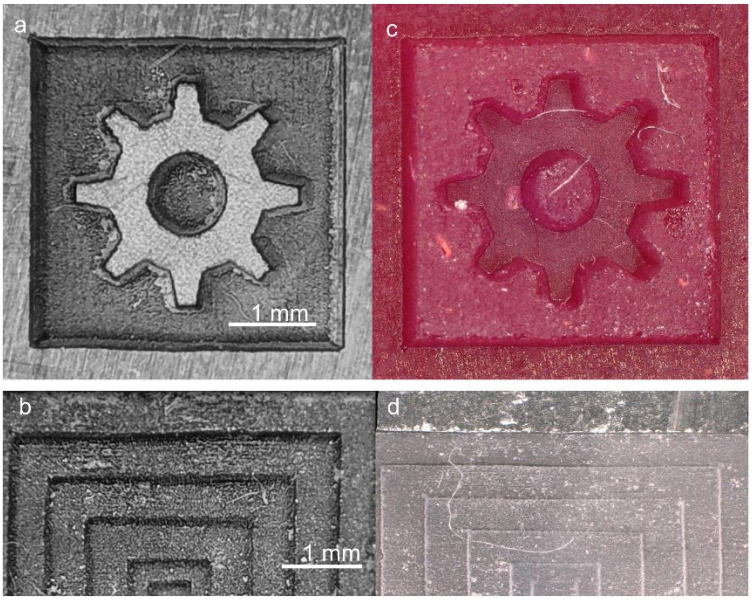

Figure 4-9. (a and b) microstructure molds, (c and d) PDMS parts taken from the molds

4.2 Summary

In this chapter, a laser micromachining method was presented to fabricate 3D microstructures. A galvoscanner for moving the laser beam in the x and y-axis and an adjustable stage in the z-axis was used to equip the setup for 3D laser micromachining. The stage repositioned the sample at the focal plane for deeper micromachining after each layer of machining.

Firstly, a pyramid shape was machined to evaluate the feasibility of the presented micromachining technique. The pyramid was machined in multiple square-shape layers and in each step the dimension of the square decreased by 1mm. This experiment was performed twice with two different laser powers of 1.1 and 2.4 W. The laser micromachining system had a good performance in fabrication of 3D pyramid in both laser powers such as machining accuracy and machining depth. The depth and roughness of the pyramids were measured by the confocal microscopy.

The laser ablation produces debris in the machining zone, which can block the laser beam to penetrate to the bottom of the grooves and prevents the deeper machining. Therefore, a 3-bar air jet was applied simultaneously to the machining area to improve the surface quality. The airflow pushed away the debris created in the grooves for better laser penetration. Moreover, the air jet decreases the temperature at the machining area which improves the machining quality and reduces the production of recast layers in the microstructure's edges.

Another experiment was designed to evaluate the laser micromachining accuracy in the creation of 3D microstructures. A gear-shape was chosen for 3D laser micromachining with two laser powers of 1.1 and 2.4 W. The results show that the laser micromachining system had a high precision performance to generate the microstructure features such as corners, inner and outer curves, and the edges.

Finally, since the aim of this study is to fabricate the 3D micro-mold, samples were poured by PDMS to create micro-parts. Then, a digital microscope was used for imaging the PDMS micro-parts. As is clear, the micrometric features such as corners, edges, and curves were accurately fabricated.

CHAPTER 5. CONCLUSION AND FUTURE WORK

5.1 Conclusion

In the first chapter, a literature review was conducted on different laser-based and non-laser-based micromachining techniques. In non-laser-based micromachining, a review on different methods such as electrochemical micromachining (ECMM), waterjet micromachining (AWJ/SAWS), bulk micromachining (wet and dry etching), and micro-texturing was conducted which have their own advantages and disadvantages.

In the laser-based micromachining section, a review of different laser micromachining methods was conducted. Laser micromachining offers higher precision, lower manufacturing costs, etc., than the other micromachining techniques. Adding different assistance to laser helped to improve the micromachining features such as surface quality, machining accuracy. Moreover, it was specified that lasers with a shorter pulse duration like pico/femtosecond lasers increase the machining quality significantly.

In the last part of the literature review, a criticism on different 3D laser micromachining systems was conducted. The literature review revealed that laser parameters have a significant effect on the quality and accuracy of 3D micromachining. There were several machining assistance techniques reviewed including argon gas, ultrasonic, and water jet, which were used to improve surface roughness and quality. Furthermore, hybrid micromachining methods, like micro-electric discharge machining (micro EDM) and wet etching, were overviewed, which are used after laser micromachining to improve surface finish. From the review, the gap the literature was identified, and the objectives of this work was formulated.

In Chapter two, the required optical components for performing laser micromachining and methods of experiments were presented. A Q-switched Nd:YVO_4 Diode Pumped Solid-State (DPSS) laser with a wavelength of 532 nm and a pulse duration of <20 ns was used in this setup. Also, a high-speed scanning galvoscanner (THORLABS GVS002) was used to control the movement of laser beam in the x and y-directions. A converging lens with a diameter of 50 mm that has been placed 200 mm (at the focal plane of the lens) away from the galvanometer mirrors. Furthermore, an adjustable stage was used to move the sample in z-direction towards the focal length to enable the 3D micromachining.

A MATLAB algorithm has been developed to control the movement of the galvoscanner mirrors, read the image, scale it, convert it to a binary image for micromachining. Since magnesium (Mg) has enormous application, it was selected as a sample for this study. In addition, an air jet was directed to the machining area during the laser micromachining to reduce the production of debris.

Evaluation of the laser parameters such as overlap, laser power, and the number of pulses was conducted to find the optimum parameters for the laser micromachining. In this study, all the experiments were performed with laser powers of 1.1 W and 2.4 W, overlaps of 0%, 40%, and 80%, and the number of pulses of 50, 100, 200, 400, and 4000 pulse/spot. Two level design of experiments was conducted to optimize these parameters for micromachining. Finally, all samples were investigated by using the white light interferometer to measure the machining depth, machining accuracy, and surface roughness. From the analysis it was found that machining with 80% overlap and 400 pulse per spot provided low surface roughness, smooth edges, and maximum depth in both 1.1 and 2.4 W laser power. These parameters were used in the 2D and 3D micromachining.

A complex 2D micromachining was designed to evaluate our laser micromachining system accuracy in generating the small features. The Concordia University logo was selected as a complex shape to be machined. Four different sizes were used between 4 to 1mm. When the logo was 1mm in size the features were not accurate as the smallest dimension at this scale becomes smaller than spot size which is 60 µm. The samples were investigated by using confocal microscope, and it was found that the average surface roughness and the depth did not have significant change within the different sizes.

A pyramid shape was micromachined in multiple layers to investigate the feasibility of 3D laser micromachining. The micromachining was performed in five different layers with the overlaps of 80%, the number of pulses of 400 pulse/spot, and two laser powers of (1.1-2.4) W. Finally, the samples were carefully investigated by interferometer and confocal microscope to identify the machining depths, surface roughness in each step. Five steps with an average depth of 195.03 ±29.32 µm.

Subsequently, a gear was selected as a complex shape to evaluate the laser micromachining accuracy in creating of 3D microstructures. The experiment was performed with the overlaps of

80%, the number of pulses of 400 pulse/spot, and two powers of 1.1 and 2.4 W. the samples were studied by interferometer microscope carefully.

In the last part of this study, the 3D microstructures were molded by PDMS. The filled-out samples with PDMS were placed into the vacuum chamber for 15 min to remove the created bubble. Then, the samples were cured in the oven at 70° for 2 hours. Finally, the PDMS were removed from the mold as a final product. The micrometric features such as corners and edges were accurately fabricated. Furthermore, the surface roughness of the machining area and the edges recast layers can affect the roughness of the PDMS structures. These results show that the approach presented in this study can be an affordable and less laborious alternative for fabrication microfluidics, etc.

5.2 Future Works

While the primary aim of the thesis for the development of 3D laser micromachining and micro-molding was successfully met, a lot of potential exists for future directions. Some of the possibilities are summarized below.

- Various materials, such as gray cast iron, which is a common material for manufacturing dies can be used as micromachining substrates.
- It is also possible to machine more complex shapes, such as curvature surfaces.
- Hybrid micromachining systems like laser-assisted chemical etching, etc., can be used to have better control over surface roughness.
- Instead of image processing, a CAD file can be prepared to be machined through laser micromachining for the fabrication of 3D complex shapes.
- Intensity-based machining approach: controlling the number of pulses by the intensity of the image, darker portions for deeper micromachining.

CHAPTER 6. REFERENCES

[1] P. Piljek, Z. Keran, and M. Math, "Micromachining," *Interdiscip. Descr. Complex Syst.*, vol. 12, no. 1, pp. 1–27, 2014, doi: 10.7906/indecs.12.1.1.

[2] S. Z. Chavoshi and X. Luo, "Hybrid micro-machining processes : A review," *Precis. Eng.*, vol. 41, pp. 1–23, 2015, doi: 10.1016/j.precisioneng.2015.03.001.

[3] K. K. Saxena, J. Qian, and D. Reynaerts, "A review on process capabilities of electrochemical micromachining and its hybrid variants," *Int. J. Mach. Tools Manuf.*, vol. 127, no. January, pp. 28–56, Apr. 2018, doi: 10.1016/j.ijmachtools.2018.01.004.

[4] S. Maniraj and R. Thanigaivelan, "Effect of electrode heating on performance of electrochemical micromachining," *Mater. Manuf. Process.*, vol. 34, no. 13, pp. 1494–1501, Oct. 2019, doi: 10.1080/10426914.2019.1655153.

[5] Y. Yuan *et al.*, "Electrochemical Micromachining under Mechanical Motion Mode," *Electrochim. Acta*, vol. 183, pp. 3–7, 2015, doi: 10.1016/j.electacta.2015.04.046.

[6] K. Xu, Y. Zeng, P. Li, and D. Zhu, "Study of surface roughness in wire electrochemical micro machining," *J. Mater. Process. Technol.*, vol. 222, pp. 103–109, Aug. 2015, doi: 10.1016/j.jmatprotec.2015.03.007.

[7] X. Liu, Z. Liang, G. Wen, and X. Yuan, "Waterjet machining and research developments: a review," *Int. J. Adv. Manuf. Technol.*, vol. 102, no. 5–8, pp. 1257–1335, Jun. 2019, doi: 10.1007/s00170-018-3094-3.

[8] D. S. Miller, "Micromachining with abrasive waterjets," *J. Mater. Process. Technol.*, vol. 149, no. 1–3, pp. 37–42, 2004, doi: 10.1016/j.jmatprotec.2004.02.041.

[9] H.-T. Liu, "Waterjet technology for machining fine features pertaining to micromachining," *J. Manuf. Process.*, vol. 12, no. 1, pp. 8–18, Jan. 2010, doi: 10.1016/j.jmapro.2010.01.002.

[10] A. Misra, J. D. Hogan, and R. Chorush, "Wet and Dry Etching Materials," in *Handbook of Chemicals and Gases for the Semiconductor Industry*, no. 3, Hoboken, NJ, USA: John Wiley & Sons, Inc., 2002, pp. 1–5.

[11] Shubhava, A. Jayarama, G. K. Kannarpady, S. Kale, S. Prabhu, and R. Pinto, "Chemical etching of glasses in hydrofluoric Acid: A brief review," *Mater. Today Proc.*, no. xxxx, Dec. 2021, doi: 10.1016/j.matpr.2021.12.110.

[12] S. S. Yoon, Y. B. Lee, and D. Y. Khang, "Etchant wettability in bulk micromachining of Si by metal-assisted chemical etching," *Appl. Surf. Sci.*, vol. 370, pp. 117–125, 2016, doi: 10.1016/j.apsusc.2016.02.153.

[13] T. K. Kim, J.-H. Bae, J. Kim, Y.-C. Kim, S. Jin, and D. W. Chun, "Bulk Micromachining of Si by Annealing-Driven Magnetically Guided Metal-Assisted Chemical Etching," *ACS Appl. Electron. Mater.*, vol. 2, no. 1, pp. 260–267, Jan. 2020, doi: 10.1021/acsaelm.9b00746.

[14] S. Hoshian, C. Gaspar, T. Vasara, F. Jahangiri, V. Jokinen, and S. Franssila, "Non-lithographic silicon micromachining using inkjet and chemical etching," *Micromachines*, vol. 7, no. 12, pp. 1–9, 2016, doi: 10.3390/mi7120222.

[15] D. Patel, V. Jain, and J. Ramkumar, "Micro texturing on metallic surfaces: State of the art," *Proc. Inst. Mech. Eng. Part B J. Eng. Manuf.*, vol. 232, no. 6, pp. 941–964, May 2018, doi: 10.1177/0954405416661583.

[16] J. D. Abou Ziki, T. Fatanat Didar, and R. Wüthrich, "Micro-texturing channel surfaces on glass with spark assisted chemical engraving," *Int. J. Mach. Tools Manuf.*, vol. 57, pp. 66–72, Jun. 2012, doi: 10.1016/j.ijmachtools.2012.01.012.

[17] S. Dongre, A. Gujrathi, and H. Nandan, "A Review of Laser Micromachining," *Int. J. Eng. Sci. Comput.*, vol. 6, no. 3, pp. 2416–2420, 2016, doi: 10.4010/2016.574.

[18] J. Lehr and A.-M. Kietzig, "Production of homogenous micro-structures by femtosecond laser micro-machining," *Opt. Lasers Eng.*, vol. 57, pp. 121–129, Jun. 2014, doi: 10.1016/j.optlaseng.2014.01.012.

[19] W. Charee, V. Tangwarodomnukun, and C. Dumkum, "Ultrasonic-assisted underwater laser micromachining of silicon," *J. Mater. Process. Technol.*, vol. 231, pp. 209–220, May 2016, doi: 10.1016/j.jmatprotec.2015.12.031.

[20] Y.-J. Chang, "Magnetic Assisted Laser Micromachining for Highly Reflective Metals," *J.*

Laser Micro/Nanoengineering, vol. 7, no. 3, pp. 254–259, Nov. 2012, doi: 10.2961/jlmn.2012.03.0004.

[21] R. Chkalov, K. Khorkov, and D. Kochuev, "Femtosecond Laser Micromachining of Metal Thin Films," *Mater. Today Proc.*, vol. 11, pp. 441–445, 2019, doi: 10.1016/j.matpr.2019.01.010.

[22] R. De Loor, "Polygon Scanner System for Ultra Short Pulsed Laser Micro-Machining Applications," *Phys. Procedia*, vol. 41, pp. 544–551, 2013, doi: 10.1016/j.phpro.2013.03.114.

[23] B. K. Nayak, P. O. Caffrey, C. R. Speck, and M. C. Gupta, "Superhydrophobic surfaces by replication of micro/nano-structures fabricated by ultrafast-laser-microtexturing," *Appl. Surf. Sci.*, vol. 266, pp. 27–32, Feb. 2013, doi: 10.1016/j.apsusc.2012.11.052.

[24] M. Martínez-Calderon *et al.*, "Surface micro- and nano-texturing of stainless steel by femtosecond laser for the control of cell migration," *Sci. Rep.*, vol. 6, no. 1, p. 36296, Dec. 2016, doi: 10.1038/srep36296.

[25] C.-W. Chang, C.-Y. Chen, T.-L. Chang, C.-J. Ting, C.-P. Wang, and C.-P. Chou, "Sapphire surface patterning using femtosecond laser micromachining," *Appl. Phys. A*, vol. 109, no. 2, pp. 441–448, Nov. 2012, doi: 10.1007/s00339-012-7048-6.

[26] C. I. Park, Y. Wei, M. Hassani, X. Jin, J. Lee, and S. S. Park, "Low power direct laser-assisted machining of carbon fibre-reinforced polymer," *Manuf. Lett.*, vol. 22, pp. 19–24, Oct. 2019, doi: 10.1016/j.mfglet.2019.10.001.

[27] J.-Y. Cheng, M.-H. Yen, C.-W. Wei, Y.-C. Chuang, and T.-H. Young, "Crack-free direct-writing on glass using a low-power UV laser in the manufacture of a microfluidic chip," *J. Micromechanics Microengineering*, vol. 15, no. 6, pp. 1147–1156, Jun. 2005, doi: 10.1088/0960-1317/15/6/005.

[28] R. Bathe, V. Sai Krishna, S. K. Nikumb, and G. Padmanabham, "Laser surface texturing of gray cast iron for improving tribological behavior," *Appl. Phys. A*, vol. 117, no. 1, pp. 117–123, Oct. 2014, doi: 10.1007/s00339-014-8281-y.

[29] M. M. Mathew, R. N. Bathe, G. Padmanabham, R. Padmanaban, and S. Thirumalini, "A

study on the micromachining of molybdenum using nanosecond and femtosecond lasers," *Int. J. Adv. Manuf. Technol.*, vol. 104, no. 9–12, pp. 3239–3249, Oct. 2019, doi: 10.1007/s00170-017-1454-z.

[30] Y. L. Yao, H. Chen, and W. Zhang, "Time scale effects in laser material removal: a review," *Int. J. Adv. Manuf. Technol.*, vol. 26, no. 5–6, pp. 598–608, Sep. 2005, doi: 10.1007/s00170-003-2026-y.

[31] K. K. Mandal, A. S. Kuar, and S. Mitra, "Experimental investigation on laser micro-machining of Al 7075 Alloy," *Opt. Laser Technol.*, vol. 107, pp. 260–267, Nov. 2018, doi: 10.1016/j.optlastec.2018.05.017.

[32] Y. Xing, L. Liu, X. Hao, Z. Wu, P. Huang, and X. Wang, "Micro-channels machining on polycrystalline diamond by nanosecond laser," *Opt. Laser Technol.*, vol. 108, pp. 333–345, Dec. 2018, doi: 10.1016/j.optlastec.2018.07.024.

[33] H.-K. Lin, C.-J. Lee, T.-T. Hu, C.-H. Li, and J. C. Huang, "Pulsed laser micromachining of Mg–Cu–Gd bulk metallic glass," *Opt. Lasers Eng.*, vol. 50, no. 6, pp. 883–886, Jun. 2012, doi: 10.1016/j.optlaseng.2012.01.003.

[34] B. Kang, G. Woo Kim, M. Yang, S.-H. Cho, and J. K. Park, "A study on the effect of ultrasonic vibration in nanosecond laser machining," *Opt. Lasers Eng.*, vol. 50, no. 12, pp. 1817–1822, Dec. 2012, doi: 10.1016/j.optlaseng.2012.06.013.

[35] D. Teixidor, T. Thepsonthi, J. Ciurana, and T. Özel, "Nanosecond pulsed laser micromachining of PMMA-based microfluidic channels," *J. Manuf. Process.*, vol. 14, no. 4, pp. 435–442, Oct. 2012, doi: 10.1016/j.jmapro.2012.09.001.

[36] V. Tangwarodomnukun, S. Mekloy, C. Dumkum, and A. Prateepasen, "Laser micromachining of silicon in air and ice layer," *J. Manuf. Process.*, vol. 36, no. September 2017, pp. 197–208, Dec. 2018, doi: 10.1016/j.jmapro.2018.10.008.

[37] R. R. Behera, M. R. Sankar, P. K. Baruah, A. K. Sharma, and A. Khare, "Experimental investigations of nanosecond-pulsed Nd:YAG laser beam micromachining on 304 stainless steel," *J. Micromanufacturing*, vol. 1, no. 1, pp. 62–75, May 2018, doi: 10.1177/2516598418766937.

[38] A. Piqué, R. C. Y. Auyeung, H. Kim, N. A. Charipar, and S. A. Mathews, "Laser 3D micro-manufacturing," *J. Phys. D. Appl. Phys.*, vol. 49, no. 22, p. 223001, Jun. 2016, doi: 10.1088/0022-3727/49/22/223001.

[39] C. Liu, X. Fu, Y. Wu, F. Sun, and X. Hu, "Ultraviolet nanosecond pulse laser 3D micro-fabrication system," pp. 178–181.

[40] Y. Huang, X. Wu, H. Liu, and H. Jiang, "Fabrication of through-wafer 3D microfluidics in silicon carbide using femtosecond laser," *J. Micromechanics Microengineering*, vol. 27, no. 6, p. 065005, Jun. 2017, doi: 10.1088/1361-6439/aa68cb.

[41] D. H. Kam and J. Mazumder, "Three-dimensional biomimetic microchannel network by laser direct writing," *J. Laser Appl.*, vol. 20, no. 3, pp. 185–191, Aug. 2008, doi: 10.2351/1.2955485.

[42] S. Kim, B. H. Kim, D. K. Chung, H. S. Shin, and C. N. Chu, "Hybrid micromachining using a nanosecond pulsed laser and micro EDM," *J. Micromechanics Microengineering*, vol. 20, no. 1, p. 015037, Jan. 2010, doi: 10.1088/0960-1317/20/1/015037.

[43] M. R. H. Knowles, G. Rutterford, D. Karnakis, T. Dobrev, P. Petkov, and S. Dimov, "Laser micro-milling of ceramics, dielectrics and metals using nanosecond and picosecond lasers," in *4M 2006 - Second International Conference on Multi-Material Micro Manufacture*, Elsevier, 2006, pp. 131–134.

[44] C. Liu, X. Fu, Y. Wu, Y. Li, F. Sun, and X. Hu, "Realization of nanosecond pulse laser micromachining system," *J. Vac. Sci. Technol. B Microelectron. Nanom. Struct.*, vol. 27, no. 3, p. 1319, 2009, doi: 10.1116/1.3119676.

[45] P. Heyl, T. Olschewski, and R. W. Wijnaendts, "Manufacturing of 3D structures for micro-tools using laser ablation," *Microelectron. Eng.*, vol. 57–58, pp. 775–780, Sep. 2001, doi: 10.1016/S0167-9317(01)00485-3.

[46] A. Žemaitis, M. Gaidys, P. Gečys, G. Račiukaitis, and M. Gedvilas, "Rapid high-quality 3D micro-machining by optimised efficient ultrashort laser ablation," *Opt. Lasers Eng.*, vol. 114, no. October 2018, pp. 83–89, Mar. 2019, doi: 10.1016/j.optlaseng.2018.11.001.

[47] Y. Wang, Z. Zhang, G. Zhang, B. Wang, and W. Zhang, "Study on immersion waterjet

assisted laser micromachining process," *J. Mater. Process. Technol.*, vol. 262, no. 1219, pp. 290–298, Dec. 2018, doi: 10.1016/j.jmatprotec.2018.07.004.

[48] S. Fang, V. Pérez, N. Salán, D. Baehre, and L. Llanes, "Surface Patterning of Cemented Carbides by Means of Nanosecond Laser," *Mater. Manuf. Process.*, vol. 35, no. 2, pp. 123–129, Jan. 2020, doi: 10.1080/10426914.2019.1628268.

[49] K. Sugioka, Y. Hanada, and K. Midorikawa, "Three-dimensional femtosecond laser micromachining of photosensitive glass for biomicrochips," *Laser Photon. Rev.*, vol. 4, no. 3, pp. 386–400, Apr. 2010, doi: 10.1002/lpor.200810074.

[50] B. . Mordike and T. Ebert, "Magnesium," *Mater. Sci. Eng. A*, vol. 302, no. 1, pp. 37–45, Apr. 2001, doi: 10.1016/S0921-5093(00)01351-4.